The antimicrobial peptide cathelicidin and polymyxin B neutralize endotoxins by a multifactorial mechanism including not only direct LPS-interaction but also targeting of host cell membrane domains

Andra B. Schromm[1*], Laura Paulowski[1,2], Yani Kaconis[2], Franziska Kopp[1,2], Max Koistinen[2], Annemarie Donoghue[2], Susanne Keese[1], Christian Nehls[2], Julia Wernecke[2,3], Patrick Garidel[4], Eva Sevcsik[5], Karl Lohner[6], Susana Sanchez-Gomez[6], Guillermo Martinez-de-Tejada[7,8], Klaus Brandenburg[2], Mario Brameshuber[5], Gerhard J. Schütz[5], Jörg Andrä[2,9], Thomas Gutsmann[2]

Publisher version: https://doi.org/10.1073/pnas.2101721118

Affiliations:

[1]Division of Immunobiophysics, Research Center Borstel, Leibniz Lung Center, D-23845 Borstel, Germany
[2]Division of Biophysics, Research Center Borstel, Leibniz Lung Center, D-23845 Borstel, Germany
[3] Deutsches Elektronen-Synchrotron DESY, D-22607 Hamburg, Germany
[4] Universität Halle-Wittenberg, D-06108, Halle/Saale, Germany
[5]Institute of Applied Physics, TU Wien, Vienna, 1040, Austria
[6]Institute of Molecular Biosciences, Biophysics Division, University of Graz, NAWI Graz, A-8010 Graz, Austria; BioTechMed-Graz, Austria
[7]Department of Microbiology and Parasitology, University of Navarra, E-31008 Pamplona, Spain
[8]Navarra Institute for Health Research (IdiSNA), E-31008 Pamplona, Spain
[9]Department of Biotechnology, Faculty of Life Sciences, Hamburg University of Applied Sciences, D-21033 Hamburg, Germany
*Correspondence: aschromm@fz-borstel.de (A.B.S.)

Classification: BIOLOGICAL SCIENCE (Biophysics and Computational Biology, Immunology and Inflammation)

Keywords: antimicrobial peptides, endotoxin, membrane biophysics, macrophages, inflammation

Author contributions: A.B.S, J.A, and T.G. conceived the project, planned, partially performed and supervised the experiments, and interpreted the data. L.P performed and analyzed the HEK cell experiments. F.K. performed the confocal microscopy, ultracentrifugation, and peptide-binding studies and the data analyses. A.D. measured the LPS surface potential. Y.K., E.S., J.A., L.P., J.W, and K.L. performed and analyzed SAXS and XRR measurements. P.G. performed DSC. Y.K. and C.N. performed AFM measurements. M.K. and L.P. analyzed peptide binding to GUV. S.K. performed gene expression studies. M.B. and G.J.S. performed and analyzed the TOCCSL experiments. S.S.G., G.M.T, J.A., and K.B. planned and performed the *in vivo* mouse model of LPS-induced sepsis. A.B.S. wrote the manuscript, with contributions from all authors. All authors read, discussed, and concurred with the final version of the manuscript.

Declaration of Interests: K.B. holds a patent for Aspidasept® and is the CEO of Brandenburg Antiinfectiva GmbH. The authors declare no competing financial interests.

This pdf includes: Main Text
Figures 1-7
Supplementary Information

ABSTRACT

Antimicrobial peptides (AMPs) contribute to an effective protection against infections. The antibacterial function of AMPs depends on their interactions with microbial membranes and lipids, such as lipopolysaccharide (LPS; endotoxin). Hyper-inflammation induced by endotoxin is a key factor in bacterial sepsis and many other human diseases. Here, we provide a comprehensive profile of peptide-mediated LPS neutralization by systematic analysis of the effects of a set of AMPs and the peptide antibiotic polymyxin B (PMB) on the physico-chemistry of endotoxin, macrophage activation and lethality in mice. Mechanistic studies revealed that the host defense peptide LL-32 and PMB reduce LPS-mediated activation also via a direct interaction of the peptides with the host cell. As biophysical basis, we demonstrate modifications of the structure of cholesterol-rich membrane domains and the association of GPI-anchored proteins. Our discovery of a host cell-directed mechanism of immune control contributes a completely novel aspect in the development and therapeutic use of AMPs.

SIGNIFICANCE STATEMENT

Antibiotics resistances among clinically relevant bacteria present an increasing threat and raises the urgent need for new compounds. Antimicrobial peptides (AMPs) and peptide antibiotics are potent membrane-active molecules and valuable prototypes for drug development. In Gram-negative infections, killing of bacteria by antimicrobials is accompanied by the release of lipopolysaccharide (LPS), an endotoxin that causes severe hyperinflammation and pathology. We demonstrate how two medical relevant peptides, the cathelicidin LL-32 and polymyxin B, disarm endotoxins by peptide-LPS interaction. Furthermore, our studies reveal a new mechanism of peptide-mediated immune control by acting on signaling domains of the immune cell membrane. Our results significantly enhance our understanding of how peptide antibiotics can regulate inflammation and will be important for the development and therapeutic use.

INTRODUCTION

Antimicrobial peptides (AMPs), a central part of the innate immune system, represent a phylogenetically conserved mechanism of immune defense in species ranging from bacteria and yeast to mammals. In humans, AMPs are found at all body interfaces, including the skin and mucosal surfaces of the lung, intestine, and urogenital tract where they provide efficient first-line protection against environmental pathogens and naturally acquired microbiota. The broad contributions of AMPs to human immune defenses against infections are exemplified by cathelicidin (1-3).

Since their introduction into medical practice, antibiotics have become indispensable for treating infectious diseases and have saved millions of lives. However, this option is largely past its prime because the potencies of these drugs have been reduced severely. The coincidence of stagnating efforts toward new antibiotic development for more than a decade (4) and the emergence of antibiotic-resistant strains of clinically relevant pathogens have led to a lack of effective antibacterial treatment options. Particularly, multi-drug resistant pathogens represent a major challenge for clinicians and hospitals (5). Notably, AMPs have long been used and optimized evolutionarily for efficiency and applicability in the human body. The success of this evolutionary process is demonstrated by the low emergence of microbial resistance to this class of defense molecules. Accordingly, AMPs represent an ideal alternative to conventional antibiotics in the development of new therapeutics against infectious diseases (6, 7).

AMPs mainly exert direct antibacterial activity, although the increasing recognition of other biological activities (8, 9) has led to the description of these molecules as host defense peptides. Particularly, AMPs play key roles in wound healing and repair by modulating immune responses

and angiogenesis. The ability to modulate inflammation in the context of infection represents a central step in the avoidance of excessive immune-mediated damage and devastating consequences such as sepsis-related multi-organ failure, shock, and death (10). Dysregulated AMP expression has been linked to several diseases associated with high morbidity (11), including Crohn's disease (CD) (12), cystic fibrosis (CF) (13), chronic obstructive pulmonary disease (COPD), and asthma (14, 15). These pathologies are driven by chronic or recurrent uncontrollable inflammatory responses.

AMPs are small (length: 20–40 amino acids) and structurally diverse (α-helical, β-sheet, circular) peptides that share a common structural motif with a strong amphiphilic nature and a net cationic charge. This particular structure forms the basis of their antimicrobial activity, which targets bacterial membranes and induces dysfunction via pore formation, membrane thinning, or lipid segregation (16). The simple and highly efficient lytic specificity of AMPs depends on charge selectivity for anionic lipids in the microbial membrane, such that the neutral surfaces of host cells are largely unaffected (17, 18). Some antibiotic peptides, such as colistin and other clinically used polymyxins, efficiently also exploit this bactericidal mechanism. However, the therapeutic potential of this immune-modulating activity is hindered by our limited understanding of the molecular mechanism.

The effects of AMPs on host cells have been attributed to the binding of AMPs to cellular receptors or intracellular targets (19-21); however, the detailed mechanisms remain unclear. Consequently, we analyzed a panel of AMPs from different molecular classes: the cathelicidin LL-37 (8) and short-variant LL-32; hBD-3-l, a variant of the β-defensin hBD-3; NK-2, a derivative of the lymphocytic effector protein NK-lysin; Pep19-2.5 (Aspidasept®), a *de novo* designed peptide (22);

and polymyxin B (PMB), a peptide-based antibiotic which binds highly specific to LPS and leads to its aggregation (23)that has been used widely in studies of LPS bioactivity neutralization. Particularly, we analyzed the effects of LL-32 and PMB on the host cell response to lipopolysaccharide (LPS; endotoxin), the main molecular trigger for the immune detection of Gram-negative infection. LPS induces severe hyperinflammatory responses and is one of the most potent inducers of sepsis and septic shock (10, 24). LPS activates immune cells via a complex interplay of transport and receptor proteins. Specifically, its recognition by the TLR4/MD-2 receptor complex on the cytoplasmic membrane (25-28) initiates several intracellular signaling cascades, leading to the production of pro-inflammatory mediators such as TNF-α, IL-6, and IL-8 (29). This recognition is strongly enhanced by the transport of LPS via LPS-binding protein (LBP) and soluble CD14 to the TLR4/MD-2 receptor complex, which enables the recognition of picogram amounts of LPS by monocytes and macrophages (30-32).

Our analyses of the effects of LL-32 and PMB on different stages of LPS-induced cell activation revealed that the AMP and PMB interact with LPS and induce structural and biophysical changes that reduce the bioactivity of this endotoxin. Changes in the aggregate structure of LPS by cationic and amphiphilic molecules has been discussed for polymers and peptides (33, 34). Moreover, we discovered specific interactions of cathelicidin AMPs and PMB with host cell cytoplasmic membranes, as well as effects of the peptides on signaling domain membrane organization. Our findings indicate a novel host cell-directed mechanism by which antibiotic peptides restrain pro-inflammatory immune responses.

RESULTS

LL-32 and PMB reduce LPS-induced inflammation *in vitro* and *in vivo*

Initially, we analyzed the potential abilities of various AMPs and PMB to reduce the pro-inflammatory responses of human macrophages to LPS. The preincubation of macrophages with the peptides at concentrations of 1–20 μM for 30 min reduced or even abolished the LPS-induced production of TNF-α (Figure 1a). Specifically, LPS-mediated cell activation was abrogated fully by LL-32 at 10 μM and Pep19-2.5 at 20 μM and inhibited by 58% and 20.7% in response to 10 μM NK-2 or hBD-3-l, respectively, and by 64.5% and 47.9% in response to 20 μM concentrations of the latter peptides, respectively. Notably, PMB exhibited the most potent activity and abrogated TNF-α production at 1 μM. Consequently, we focused on LL-32 and PMB as the most potent peptides in subsequent analyses.

We next induced a mouse model of endotoxin shock via the intravenous injection of LPS into the bloodstream. In the saline control group, 87.5% of the animals died within 4 days of LPS injection. The administration of LL-32 or PMB rescued the mice from lethal LPS-induced sepsis *in vivo* (Figure 1b). The survival rate increased to 75% after treatment with LL-32 (100 μg/mouse) and was maintained at 100% after treatment with PMB (100 μg/mouse). These results demonstrate the effective ability of these peptides to reduce the exaggerated immune response to endotoxin.

The LPS-neutralizing activities of these cationic peptides have been attributed to strong interactions with the negatively charged LPS molecule and subsequent physicochemical changes in the LPS structure (35). To differentiate whether the observed immunomodulatory functions of AMPs are based on the neutralization of LPS or on the modulation of host cell functions, we performed

126 washing experiments in which human macrophages were incubated with the peptides for 30 min
127 at 37°C and washed to remove free peptide prior to LPS stimulation. We observed that the
128 preincubation of macrophages with the peptides leads to a significant reduction (LL-32 **$p \leq 0.01$,
129 PMB ***$p \leq 0.001$ peptide versus LPS control) in LPS-mediated TNF-α production, even if the
130 cells were washed intensively before stimulation with LPS (Figure 1c). These data suggest that the
131 anti-inflammatory effects of the peptides are not solely dependent on LPS neutralization via direct
132 peptide binding, but also rely on interactions between peptides and the host cell. Accordingly, our
133 flow cytometry data reveal the dose-dependent binding of fluorophore-conjugated LL-32 and PMB
134 to human macrophages (Figure 2a; see Figure S1 for the gating strategy). The results of our
135 fluorescence quenching assay with trypan blue demonstrated that considerable proportions of both
136 LL-32 and PMB were not internalized but remained exposed on the cell surface. In contrast,
137 Pep19-2.5 exhibited very low binding to macrophage membranes.
138
139 We next characterized the effects of the peptides on different stages of host cell activation. Both
140 LL-32 (Figure 2b) and PMB (Figure S2) reduce but do not completely abrogate the binding and
141 internalization of LPS by human macrophages. A confocal microscopy analysis further
142 demonstrated the condensing effect of LL-32 on the intracellular LPS pool, an observation that
143 could be relevant for the activation of intracellular LPS-receptors such as caspase-4, -5, and -11
144 (36). As shown in Figure 2c, larger intracellular LPS aggregates are visible at LL-32 concentrations
145 of 3 and 10 µM. Moreover, the peptides affected the production of inflammatory mediators by
146 human macrophages at the transcriptional and translational levels. Specifically, LL-32 attenuated
147 the transcriptional activation of the pro-inflammatory cytokines TNF-α and IL-1β and the
148 chemokine IL-8 at 1 µM and suppressed this expression at 3 and 10 µM. PMB yielded similar
149 results (Figure 2d). A similar dose-dependent effect of AMPs on intracellular TNF-α was observed

(Figure 2e), demonstrating that the anti-inflammatory effects of these peptides are exerted at an early stage of activation. We did not observe any cytotoxic effects of the peptides on human macrophages or HEK293-TLR4/MD2 cells at the experimental concentrations; however, LL-32 exerted a low level of hemolytic activity against human erythrocytes (see Figure S3).

LL-32 and PMB modulate the 3D structure, surface charge, and transport of LPS

The biological activity of LPS is dependent on the aggregation state, the presentation of the two negatively charged phosphate groups on the backbone, and the overall 3D structure (37), and this activity is modified by the binding of cationic peptides and proteins to the phosphate groups. The titration of LL-32 or PMB to LPS aggregates in solution leads to a significant increase of the size of aggregates from 510 ± 47.6 nm to 906 ± 56.3 nm for LL-32 and to 999 nm ± 205.1 nm for PMB (Fig. 3a) and neutralized the negative surface charge of the LPS aggregates (zeta potential: −27 ± 4.75 mV) to varying degrees. The addition of PMB almost fully neutralized the surface charge (zeta potential: −5.2 ± 1.7 mV), whereas the addition of LL-32 induced charge overcompensation (zeta potential: +17 ± 2.2 mV; Figure 3b). This observation suggests the binding of a higher concentration of LL-32 to the membrane surface. Accordingly, the addition of LL-32 and PMB to LPS coated on a solid-support of mica induced strong changes in the lateral membrane organization, as visualized by atomic force microscopy (AFM; Figure 3c). PMB treatment yielded a smooth bilayer surface suggestive of deeper penetration of this peptide into the LPS bilayer core, whereas LL-32 accumulates on the membrane surface and formed larger irregular domains (Figure 3c). These findings are consistent with our small-angle X-ray scattering (SAXS) data (Figure 3d). Specifically, pure LPS yielded a diffuse symmetric scattering curve characteristic of the formation of unilamellar aggregates caused by the negative surface charge, which led to a net electrostatic repulsion of the LPS bilayers (38). In the presence of LL-32, the appearance of Bragg

peaks in the SAXS profile clearly indicates the formation of strongly correlated LPS bilayers, presumably due to the shielding of negative charges by the bound peptide and a consequent drastic change in the aggregation structure. In contrast, the addition of PMB did not significantly alter the shape of the scattering profile relative to pure LPS, but significantly shifted the maximum to higher angles, indicating a thinning of the LPS bilayer. This observation may be explained by partial intercalation of the peptide into the hydrophobic core, consistent with the AFM measurements (Figure 3c).

LPS-induced cell activation is enhanced greatly by LBP activity in the serum, which enables cells to respond sensitively to minute amounts of LPS (30). To determine the effects of AMPs on the LBP–LPS interaction, we incubated LPS aggregates with LBP in the presence of LL-32 or PMB and sedimented the aggregates by centrifugation before subjecting the supernatant and pellet fractions to Western blotting for LBP. Notably, LBP was detectable in the supernatant fraction (S) in the absence of LPS, but sedimented into the pellet fraction (P) when the sample was incubated with LPS aggregates, thus demonstrating the binding of LBP to LPS aggregates. The addition of an equimolar concentration of LL-32 or a 10-fold excess of PMB to the LPS aggregates strongly reduced the amount of LPS-bound LBP (Figure 3e). A densitometric analysis confirmed that LL-32 and PMB significantly reduced the binding of LBP to LPS aggregates (Figure 3f). These data are consistent with our observation that both peptides reduce the binding of LPS to cells (Figure 2b and Figure S2a,) and demonstrate their effects on LPS transport.

Inhibitory effects of LL-32 and PMB specifically impair cell activation by LPS

Primary cells, such as human macrophages, exhibit variable and strongly donor-dependent responses. Therefore, we subjected HEK293 cells expressing the TLR4/MD-2 receptor complex to

198 washing experiments. Cells washed after peptide exposure exhibited a significantly reduced ability
199 to respond to LPS (**$p \leq 0.01$, ***$p \leq 0.001$) when compared with unexposed cells (Figure 4a),
200 whereas unwashed cells exhibited enhanced peptide-mediated inhibitory activity (****$p \leq 0.0001$;
201 Figure 4b). As shown in Figure S4, this phenomenon was not restricted to LL-32 or PMB, as other
202 cathelicidin peptide family members, including the full-length peptide LL-37 (***$p \leq 0.001$), rabbit
203 fragment rCAP18 (****$p \leq 0.0001$), murine CRAMP (****$p \leq 0.0001$), and bovine BMAP-27 and
204 BMAP-28 (****$p \leq 0.0001$), strongly reduced LPS-induced pro-inflammatory activity in washing
205 experiments (Figure S4). In contrast, the NK-lysin derivative NK-2, an unrelated peptide, lacks
206 this capacity, as demonstrated by a complete loss of its endotoxin-inhibitory potential after cell
207 washing (Figure S5a and S5b). This observation demonstrates that NK-2 cannot exploit the
208 inhibitory mechanism used by cathelicidins, probably due to differences in the interactions of these
209 two types of compounds with cells and/or LPS.
210
211 To determine the ability of LL-32 or PMB to inhibit pro-inflammatory signaling cascades not
212 triggered by LPS via the TLR4/MD-2 pathway, we analyzed the effects of both peptides on cell
213 activation mediated by IL-1β (Figure 4c) and TNF-α (Figure 4d). The inability of either peptide to
214 prevent cytokine-induced cell activation suggests that the immunomodulatory mechanism
215 specifically targets the TLR4/MD-2 signaling cascade. Notably, IL-8 production in response to
216 IL-1ß-mediated cell activation was even enhanced by LL-32 and PMB, and these peptides had only
217 minor inhibitory effects on intracellular TNF-α levels (Figure S6a) or TNF-α secretion
218 (Figure S6b). This observation is particularly important, as the IL-1 and TLR4 receptors share a
219 conserved cytoplasmic domain, the Toll/IL-1 receptor homologous region (TIR), which recruits
220 the intracellular signaling adaptor MyD88 upon receptor activation.

To differentiate the direct LPS-neutralizing and immunomodulatory effects of these peptides, we compared the biological responses of cells preincubated with peptides and those treated with LPS+peptides. Both LL-32 and PMB inhibited cell activation under both conditions (Figure S5c and S5d). In contrast, the peptides NK-2, hBD-3-l, and Pep19-2.5 exhibited the most pronounced inhibitory effects only when preincubated with LPS (Figure S5c). A biophysical analysis of all investigated peptides revealed clear changes in the 3D structure of LPS as determined by the SAXS analysis of diffraction and AFM analysis of membrane organization (Figure 3b, 3c, and data not shown). These data demonstrate differences in the interactions of the peptides with LPS and with the host cell. Therefore, we suggest that LL-32 and PMB exhibit an anti-inflammatory effect via interactions with the host cell membrane, whereas other peptides neutralize LPS primarily via direct interactions.

LL-32 and PMB interact with and modify the organization of signaling domains in the host cell membrane

TLR4/MD-2 pathway signaling relies on the recruitment of the receptors into cholesterol-containing membrane domains (39, 40). We observed that the β-cyclodextrin-mediated depletion of cholesterol from HEK293-TLR4/MD-2 cells reduced the LPS-induced production of IL-8 (Figure 4e). These data, together with data from the washing and preincubation experiments, led us to investigate the effects of LL-32 and PMB on cholesterol-containing cytoplasmic membrane domains, using the well-established DOPC:sphingomyelin (SM):cholesterol (Chol) (2:2:1 molar ratio) vesicle model. We implemented giant unilamellar vesicles exhibiting phase separation to study the lateral distributions of these peptides. The low-cholesterol areas (i.e., liquid-disordered, l_d domain) of the vesicles were highlighted by a fluorescent lipid–dye, whereas the cholesterol-rich domains (liquid-ordered, l_o domain) appeared black due to exclusion of lipid–dye. The addition of

fluorophore-conjugated peptides to the vesicles revealed that the peptides interact with the phospholipid membrane with different specificities; LL-32 (l_d domains) and PMB (l_o domains) favor opposite sites of interaction on the membrane (Figure 5a, b). The biological activity of the fluorophore-conjugated peptides was only marginally reduced compared to the unconjugated peptides (Figure S6c). An evaluation of the fluorescence intensities of the fluid domain marker and peptides indicated positive and negative correlations of both signals for LL-32 and PMB, respectively.

The effects of peptides on the lateral organization of membrane domains on solid-supported bilayers composed of DOPC:SM:Chol (9:9:2 molar ratio) was investigated by AFM. The image of pure membranes demonstrates that the l_o domains are 0.74 ± 0.39 nm higher than the l_d domains; the l_o domains are smaller compared to the GUV mixture (2:2:1 molar ratio) and the interfacial effects at the domain rims are more prominent. LL-32 treatment reduced the l_o domain size, as indicated by the change in the l_d/l_o ratio from <1 to >1 after peptide addition (height histogram, Figure 5c) and by an increase in the inter-domain height difference to 3.55 ± 0.85 nm (Figure 5c). In contrast, PMB only induced slight changes in the l_o domain sizes and a marginal change in the domain height (0.82 ± 0.43 nm). These observations indicate that the two peptides interact differently with the membrane. X-ray reflectivity (XRR) experiments on solid-supported membrane stacks provide high resolution data on the membrane organization. XRR-data confirm a thickening of ordered membrane domains from 4.68 ± 0.6 nm to about 8.0 nm in the presence of LL-32 (Figure S7a) and show a stabilization of the domain structure by LL-32 even at a higher temperature of 40°C (Figure S7b). The XRR-data do not indicate changes in the membrane thickness in the presence of PMB, but they demonstrate effects of PMB on the domain structure, with more variability in membrane phases indicated by the broadening of the reflection peaks observed at 40°C (Figure S7a,b). Thermodynamic analyzes of DOPC:SM:Chol membranes did not

indicate that the interaction of PMB with the lipid system induces any relevant change in the phase transition enthalpy nor a change in the broadness of the phase transition (Figure S7c).

To account for the much more complex composition of biological membranes, we next investigated a lipid mixture closer resembling the lipid composition of macrophage membranes. AFM imaging of PL_{MAK}:SM:Chol (2:0.5:0.2 molar ratio) membranes corroborated the results obtained for LL-32. This lipid mixture is much more fluid, less-structured and the cholesterol-containing domains are much smaller. LL-32 first binds to the l_d domains and then induces a dramatic change in the domain structure leading to smaller domains with an inter-domain height difference of about 5.8 nm (Fig. 5d). Furthermore, a clear interaction of PMB with cholesterol-containing domains can be observed with this lipid mixture leading to a time-dependent height increase of about 1-3 nm. A change in domain area could not be observed.

Consequently, we characterized the effects of LL-32 and PMB on eukaryotic membranes in more detail, now with a focus on the macrophage mimetic PL_{MAK} membranes. Whereas LL-32 and PMB both demonstrate binding to PL_{MAK}:SM:Chol membranes (Figure 6a), the mode of interaction is different for the peptides. PMB dissociated from the membrane when the peptide loading was terminated at t = 6 min, whereas LL-32 remained membrane-bound. Probing the membrane surface area by a Förster-resonance-energy-transfer assay showed a dose-dependent increase of the membrane surface area consistent with membrane intercalation for LL-32, whereas no such effect was observed for PMB (Figure 6b). Analysis of a several titration experiments shows a clear increase of the membrane area for LL-32 at biological relevant doses starting at 1 µM concentration. For PMB, a significant reduction in membrane surface area is observed, supporting the conclusion that PMB binds, but does not intercalate into the membrane leaflets (Figure 6c). In line with these results, LL-32 induced a rigidification of the lipid acyl chains over a broad range of

temperatures in DOPC:SM:Chol membranes and in PL_{MAK} membranes containing various contents of cholesterol (Figure 6d), with a significant reduction of membrane fluidity at the physiological temperature 37°C (Figure 6e). In contrast, PMB does not affect the membrane fluidity in any of the lipid systems. Investigation of biological membranes using the HEK293 cell line confirmed these results also in living cells (Figure 6f).

To obtain evidence for the consequences of LL-32 and PMB membrane interaction on the organization of cholesterol-rich domains in living cells, we used a monomeric green fluorescent protein (mGFP) attached to the outer leaflet of the plasma membrane of CHO cells via a glycosylphosphatidylinositol (GPI) anchor as a model system for cholesterol-dependent protein-interactions (41). The fraction of mGFP-GPI homo-associates (α_2) was changed highly significantly after peptide addition, showing an increase after the addition of LL-32 (from 31 ± 3% to 53 ± 3%) and a decrease after addition of PMB (from 25 ± 1% to 16 ± 1%) (Figure 6a), consistent with the data from the reconstituted membrane systems. Thus, we conclude that LL-32 binds to the l_d domains and induces a domain-condensing effect, while PMB binds to the l_o domains and induces the spreading of molecules associated with cholesterol-rich domains.

DISCUSSION

Severe inflammatory diseases such as sepsis, acute respiratory distress syndrome, Crohn's disease, CF, COPD, and asthma demonstrate the impact of immune dysregulation on disease development and progression. In Gram-negative infectious diseases, the neutralization of LPS and regulation of the anti-inflammatory immune response are as important as the cytotoxic effect on bacteria. Considering this, the combined antibacterial and anti-inflammatory effects of AMPs emerge as an example of the perfect adaptation of innate immunity to these requirements.

Here, we present a new mechanism of immune modulation by members of the cathelicidin family, namely LL-32, LL-37, CAP18, CRAMP, BMAP-27/28, and the peptide antibiotic PMB, in human macrophages and human HEK293 cells. Our findings strongly suggest the multifaceted nature of the anti-inflammatory activities of these peptides, as outlined in Figure 7. Our cellular and biophysical investigations of the mechanism underlying this host cell-based immunomodulatory response identified for the first time the cytoplasmic membrane as a target of the peptides. Our DOPC:SM:Chol and macrophage mimicking PL_{MAK} model membrane experiments revealed the mode of interaction of LL-32 and PMB with the lipid matrix of the cytoplasmic membrane. In depth biophysical analysis of the structural and biophysical effects of the peptides on membrane domains revealed differential mechanism of interaction leading to subsequent changes in the membrane domain organization: LL-32 preferentially interacts with liquid-disordered domains and induces a subsequent reduction on overall membrane fluidity as well as condensation and thickening of cholesterol-containing membrane domains. We assume that this latter step is accompanied by diffusion of LL-32 into the cholesterol-containing domains, since this is currently the best model to explain the observed membrane thickening. PMB binds preferentially to the headgroup region of the liquid-ordered membrane domains. The biophysical effects are less

obvious but clearly include conversion of ordered membrane domains to smaller size as observed for the PL_{MAK} membranes, but without affecting the overall membrane fluidity. However, although LL-32 and PMB exhibited a reciprocal preference for cholesterol-containing domains, both peptides affected the organization of GPI-anchored proteins in the cytoplasmic membranes of eukaryotic cells.

The homo-association of GPI-anchored protein is a hallmark of confinement within cholesterol-dependent nanodomains (41). The LL-32-mediated increase in mGFP-GPI homo-association in the plasma membranes of live cells is consistent with the condensing effect of this peptide on cholesterol-containing domains in phase-separated model membranes, and reflects the direct dependence of protein organization on the lipid environment. *Vice versa*, the direct interaction of PMB with cholesterol-dependent membrane domains reduced the homo-association of mGFP-GPI in live cells. Thus, despite differences in domain specificity, we identified a common mechanism by which both peptides mediated changes in protein organization and association in cholesterol-dependent domains.

LPS-signaling complex activation is closely associated with dynamic TLR4 recruitment to cholesterol-containing domains upon LPS binding (39, 40). This process leads to TLR4/MD-2 homodimer formation (42, 43) and active signal transduction (29, 44-46). Currently, the exact molecular mechanisms by which the peptides modulate immune activity can only be hypothesized, although the following mechanistic scenarios for the membrane-based signaling modulation of the LPS receptor complex are plausible: The peptides i) may hinder recruitment of the TLR4 receptor via partitioning to the condensed cholesterol-containing domains in which GPI-anchored proteins are present at a higher degree of association, or ii) may hinder signaling complex assembly by

reducing the homo-association of GPI-anchored LPS receptor protein CD14 or its association with TLR4, leading to an increased activation threshold. Neither mechanism relies on a particular peptide receptor, as was demonstrated previously for some biological functions of LL-37 (47). The LPS receptor system is among the most stringently regulated innate immune receptors and employs several sensitization and deactivation circuits. The membrane-based regulation of LPS activation by cathelecidin AMPs and PMB described in this work is an entirely new anti-inflammatory mechanism.

In this study, the inability of LL-32 and PMB to inhibit IL-1β- and TNF-α-induced cell activation demonstrates the strong specificity of this new mechanism for LPS signal transduction. Although IL-1β and TNF-α receptor activation has been linked to lipid raft domains, this process does not involve the degree of dynamic receptor protein association as described above for TLR4 receptor activation. This difference may explain the lesser effects of membrane disturbances on IL-1β and TNF-α receptor signaling. IL-1 receptor type 1 (48) and TNF receptor type 1 (TNFR1) are constitutively present in lipid rafts, and a study of murine macrophages revealed that TNFR1 NF-kB signaling is not sensitive to lipid raft manipulation (49). Moreover, our data, in which LL-32 and PMB only moderately interfere with cytokine-induced cell activation, demonstrate that peptide-mediated immunomodulation does not result from a general suppression of the host immune cell response. Previous observations regarding IL-1β and TNF-α signaling in human PBMCs support our findings (50, 51). The signaling specificity reported in our work is important to the consideration of AMPs and PMB as potential antibacterial or anti-inflammatory therapeutic agents. Immunosuppression during the later phases of hyperinflammatory diseases, such as systemic infection and sepsis, is a critical driver of immune pathology (52, 53). Here, we show that exposure to LL-32 and PMB has little effect on the capacity of immune cells to respond to

385 endogenous cytokine signals. Accordingly, these peptides enable control of the immune response
386 rather than a nonspecific immunosuppressive response.
387
388 Previous studies of the interactions of AMPs with lipid bilayers have identified membrane lesions
389 or pore formation as the basis for antimicrobial activity (16). The negative aspect of this mode of
390 action is reflected by the cytotoxic effects of numerous AMPs at higher concentrations. Notably,
391 the peptides used in this study exhibited low or no cytotoxic effects on human macrophages,
392 HEK293, and red blood cells *in vitro*. We therefore conclude that host cell-directed membrane
393 interaction represents a relevant biological function, as opposed to the harmful effects of
394 cytotoxicity at higher concentrations of peptides. Our data also demonstrate that the peptides exert
395 varied effects on different domain-associated signaling cascades. We therefore assume the
396 existence of various types of membrane domains.
397 The further development of AMPs or polymyxin-based compounds as drugs for clinical use will
398 require more detailed knowledge about the modes of action of these peptides (54). Their potential
399 uses as antimicrobial agents are highly apparent, as demonstrated by the recently described new
400 class of polymyxin B-derived peptidomimetics that exhibit high potential for the treatment of
401 resistant Gram-negative pathogens of the ESKAPE group (55). Our discovery of a new peptide-
402 mediated mechanism of immune control adds a completely new aspect that will be important for
403 the development and use of antibiotic peptides for clinical use.
404
405 In conclusion, our findings reveal for the first time that the interactions of cathelicidin AMPs and
406 PMB with lipid bilayers not only provide the basis for the antimicrobial activities of these peptides
407 against bacterial membranes, but also support the host-directed modulation of the inflammatory
408 responses of immune cells. This latter function may be important in the context of acute

hyperinflammatory responses, such as bacterial sepsis, and may also be applicable to chronic hyperinflammatory diseases induced by recurrent infections, such as COPD or CF. We have demonstrated that LL-32 and PMB confer LPS neutralization via three actions: (i) modification of the agonistic LPS conformation to an antagonistic conformation, (ii) detection of LPS in serum by LBP, and (iii) modification of the receptor domain. This multi-targeted function likely explains the observed high level of activity and broad-spectrum LPS-neutralizing activity observed *in vivo*. Further studies of the host-directed functions are needed to elucidate fully the physiological impacts and therapeutic potential of AMPs and peptide antibiotics as anti-inflammatory immune response modifiers.

MATERIALS and METHODS

Reagents

Peptides were synthesized and purified by high-performance liquid chromatography (HPLC) at the peptide synthesis core facility of the Research Center Borstel. The purity of each peptide was >95% and determined from the corresponding HPLC peak. Peptide identity was confirmed by a mass spectrometry. The peptide sequences are presented in Table S1. The peptides were labeled with small fluorophores as follows. Lissamine rhodamine B or N-(7-nitrobenz-2-oxa-1,3-diazol-4-yl) was conjugated to the N-termini of synthesized LL-32 and L-Pep19-2.5 (LL-32-Rh, LL-32-NBD, Pep19-2.5-NBD). PMB (Life Technologies, Thermo Fisher Scientific), a nearly three-fold smaller cyclic lipopeptide, was conjugated to 4,4-difluoro-4-bora-3a,4a-diaza-s-indacene (BODIPY) using a newly developed protocol in which BODIPY® FL-C_5 NHS Ester (Molecular Probes, Thermo Fisher Scientific) was coupled to the free amino groups of the peptide with a C_5 carbon spacer between to yield a green fluorescent peptide (PMB-BODIPY). A mixture of mono- and di-substituted fluorescent peptides was purified by HPLC. The peptide quality was assessed by HPLC and a mass spectrometry analysis. 1,2-dioleoyl-sn-glycero-3-phosphocholine (DOPC), egg chicken L-α-phosphatidylcholine (PC), bovine liver L-α-phosphatidylethanolamine (PE), porcine brain L-α-phosphatidylserine (PS), porcine brain sphingomyelin (SM) and ovine wool cholesterol (Chol) were purchased from Avanti Polar Lipids. The lipid-dye conjugates Lissamine™ rhodamine B 1,2-dihexadecanoyl-sn-glycero-3-phosphoethanolamine (Rh-DHPE), N-(7-nitrobenz-2-Oxa-1,3-diazol-4-yl)-1,2-dihexadecanoyl-sn-glycero-3-phosphoethanolamine (NBD-PE) and β-BODIPY® FL C5-HPC (BODIPY-PC; 2-(4,4-difluoro-5,7-dimethyl-4-bora-3a,4a-diaza-s-indacene-3-pentanoyl)-1-hexa-decanoyl-sn-glycero-3-phosphocholine) were purchased from Invitrogen and Molecular Probes, respectively.

LPS aggregate preparation

Deep-rough type LPS Re was extracted from *Escherichia coli* strain WBB01 grown at 37°C (56). After extraction via the phenol/chloroform/petrol ether method, LPS was purified and lyophilized (57). Subsequently, LPS aggregate dispersions were prepared in 20 mM HEPES, 150 mM NaCl, pH 7.4 or water by applying a pulsed ultrasound (Ultrasonic-Homogenizer *HTU Soni130*, 1 min, pulse on/off: 2 s, amplitude 30%) followed by three rounds of thermocycling between 4°C and 56°C for 30 min each. Preparations were stored overnight at 4°C before use.

Macrophage model membranes

The lipid mixture resembling the composition of macrophage membranes (PL_{MAK}) was prepared by mixing the phospholipids from chloroform stocks to a final molar ratio [PC:PS:PE]:SM = 1:0.4:0.7:0.5 (M) +cholesterol 0.5 or 0.2 (M). For DOPC:SM:Chol model membranes lipids were mixed to a final ratio of (9:9:2 M) or (2:2:1 M) as indicated for the respective experiments. The organic solvent was evaporated under a stream of nitrogen until completely dry. Lipids were suspended in 20 mM HEPES, 150 mM NaCl, pH 7.4 to a final concentration of 1 mM. Liposome formation was induced by pulsed ultrasound (Ultrasonic-Homogenizer *HTU Soni130*, 1 min, pulse on/off: 2 s, amplitude 30%) followed by three rounds of thermocycling between 4°C and 56°C for 30 min each. Preparations were stored overnight at 4°C before use.

Animal model of endotoxicity

Seven-week old female C57BL/6 mice were purchased from Harlan Spain (Harlan Interfauna Iberica S.A., Barcelona, Spain) and distributed randomly in experimental groups (n = 8 per group). Endotoxemia was induced by the intraperitoneal co-administration of LPS and D-galactosamine

(18 mg/mouse), a compound that sensitizes animals to LPS (58). LPS was dissolved in endotoxin-free saline and prepared as described above. Previous experiments identified 100 ng/mouse as the LPS dose that induced 90% mortality (LD_{90}) at 48 h post-inoculation. Immediately after the injection of the LD_{90} dose of LPS, animals received an injection of either 100 or 50 µg of LL-32 dissolved in 150 µl of pyrogen-free saline at a different peritoneal site. In each experiment, one group of LPS-challenged mice received inoculations with the same amount of PMB (an effective anti-endotoxemia treatment), while the other group received only saline. To evaluate the treatment efficacy, survival was monitored at daily intervals for 96 h. Parallel survival plots were compared statistically using the log-rank test, whereas intersecting plots were compared using the Breslow-Gehan-Wilcoxon test. All p-values represent comparisons of mortality data from the same experiment (treated vs. untreated mice). All mouse experiments were approved by the University of Navarra Animal Research Committee (permission number 069/09). Animal experiments were assessed without blinding of the treatment group identity.

Stimulation of human macrophages by LPS

Human mononuclear cells (MNC) from anonymous healthy donors were isolated from heparinized peripheral blood using the Hypaque–Ficoll gradient method. The experimental use of MNC was approved by the Ethical Commission of the University of Lübeck (12-202A). All volunteer donors provided informed consent prior to the procedure. Collected MNCs were harvested, washed, and cultivated for 7 days in Teflon bags containing RPMI 1640 medium containing 100 U/ml penicillin, 100 µg/ml streptomycin, 2 mM L-glutamine, 4% heat-inactivated human AB serum, and 2 ng/ml human M-CSF for differentiating monocytes to macrophages. The cultures were incubated at 37°C in a 5% CO_2 atmosphere.

For stimulation experiments, macrophages were suspended in RPMI 1640 medium containing 100 U/ml penicillin, 100 µg/ml streptomycin, 2 mM L-glutamine, and 4% human AB serum (complete medium) and seeded into 96-well tissue culture plates at a density of 10^5 cells/well. The cells were incubated with peptides at the indicated concentrations for 30 min at 37°C and were subsequently washed three times to remove non cell-bound peptide or stimulated directly with LPS for 4 h at 37°C. Cell-free supernatants were collected and analyzed in duplicate using an OptEIA set to determine the concentration of human TNF-α (BD Biosciences). The reported data are representative of at least three independent experiments involving cells from different donors.

To detect intracellular TNF-α protein, macrophages were seeded into 5 ml Falcon tubes in RPMI 1640 complete medium containing 10 µg/ml bafilomycin to prevent protein secretion. The cells were incubated with LL-32 or PMB for 30 min at 37°C and subsequently stimulated with LPS or the cytokine IL-1 (PeproTech) at the indicated concentrations. After 4 hours, the cells were washed twice in ice-cold PBS, permeabilized in 0.1% SAP-buffer and stained with a fluorescein-conjugated antibody specific for human TNF-α (R&D Systems). A flow cytometry analysis of the cells was performed on a FACSCalibur system (BD Biosciences) using BD CellQuest software, version 6.0 (BD Biosciences). Figure S1 depicts the strategy used to gate macrophages in the MNC population. The data analysis was performed using WinMDI software (Scripps Research Institute). In each experiment, paired samples were stimulated in the absence of bafilomycin, and the concentration of secreted TNF-α protein in the supernatant was measured by ELISA. The published flow cytometry data presented are representative of three independent experiments performed using cells from different donors.

Cell lines

The HEK293-TLR4/MD2 cell line was described earlier (59) and maintained in DMEM medium (Biochrom) containing 10% low-endotoxin-grade fetal calf serum (Linaris), 100 U/ml penicillin, 100 µg/ml streptomycin, and 2 mM L-glutamine in the presence of 400 U/ml hygromycin and 0.5 mg/ml G418. Wildtype HEK293 cells were maintained in DMEM medium containing 10% low-endotoxin-grade fetal calf serum (Linaris), 100 U/ml penicillin, 100 µg/ml streptomycin, without selection antibiotics. The culture was maintained at 37°C in an atmosphere of 5% CO_2. For experiments, HEK293-TLR4/MD2 cells in DMEM medium containing 10% fetal calf serum (FCS) were seeded into 96-well plates at a density of 5×10^4 cells/well and allowed to adhere for 1 h. The peptides were diluted in 20 mM HEPES buffer (pH 7.4) and added to the wells at the indicated concentrations. After a 30 min incubation at 37°C, the cells were washed three times to remove free peptide or stimulated directly with LPS, IL-1β, or TNF-α (PeproTec) for 24 h at 37°C. For cholesterol-depletion experiments, the wells of 96-well culture plates were treated with *β*-methyl-cyclodextrin (Sigma-Aldrich) in serum-free DMEM for 1 h at 37°C. After washing, fresh DMEM containing 10% FCS was added to the plates, and the cells were stimulated with LPS as indicated. Cell-free supernatants were collected, and the concentrations of human IL-8 were analyzed in duplicate using an OptEIA set (BD Biosciences). All experiments were performed in triplicate, and the data represent the means and ±SEM of at least three independent experiments.

CHO cells (ATTC #CCL-61) that had been stably transfected with mGFP-GPI (please refer to (41) for details) were grown in DMEM/F12 medium (PAA-Laboratories) supplemented with 10% fetal calf serum (PAA-Laboratories) and 400 µg/ml G418 (PAA-Laboratories). The cells were cultured on 10 cm tissue culture plates (Greiner Bio-one) in a humidified atmosphere at 37°C and 5% CO_2. For experiments, the cells were harvested using Accutase (eBioscience), seeded into eight-well Lab-Tek chambered slides (Nunc), and allowed to reach 50% confluency on the day before

measurements. Before peptide incubation, the cells were rinsed twice with HBSS containing calcium and magnesium (PAA-Laboratories). All experiments were performed at 37°C with peptides remaining in solution.

Cell viability assays

The cytotoxicity of the tested peptides against human macrophages and HEK293-TLR4/MD-2 cells was determined using an MTT assay. The peptides were diluted from stock solutions in complete cell culture medium and incubated with the cells for 4 h (human macrophages) or 24 h (HEK293 cells) at 37°C. "Incubation time" refers to the incubation time during a stimulation experiment. Cell metabolic activity, a measure of cell viability, was determined via an additional 2 h incubation at 37°C in the presence of 5 mg/ml MTT (Sigma-Aldrich) in PBS. The reaction was terminated with stop-reagent, and the absorbance in each plate well at 570 nm (A_{570}) was analyzed photometrically. The data indicate the metabolic activity as the % viability of the control.

Human erythrocytes isolated from the blood of healthy donors were subjected to a hemolysis assay. Erythrocytes in PBS (pH 7.4) were seeded in 96-well round-bottomed plates at an $OD_{412\,nm}$ of 1.4. Peptides were diluted in PBS, added to the cells, and the cells were incubated for 30 min at 37°C. Hemolysis was determined according to the A_{405}. Hemolysis was calculated as a percentage of the control (Triton-X 100-lysed erythrocytes). Data represent the mean and ± SEM of three independent experiments performed in duplicate.

Quantitative real-time PCR (qRT-PCR)

Human macrophages were seeded in 96-well plates at a density of 5×10^5 cells/well; incubated with PMB, LL-32, or control medium for 30 min at 37°C; and subsequently stimulated with LPS. After 1 h of stimulation, the cells in each well were harvested with 200 µl FCP-buffer from the

FastLane cDNA kit (Qiagen) for RNA isolation. To generate cDNA, total RNA was isolated from the cell lysates and reverse-transcribed using the FastLane cDNA kit (Qiagen). Gene-specific primer pairs and Universal Probe Library probes (see Table S2) were obtained from Roche Diagnostics and used in a TaqMan assay. Quantitative real-time PCR amplification was performed on a LightCycler 480 II system (Roche Diagnostics). The threshold values (C_t values) were determined using LightCycler 480 software, and the relative expression ratios of the target gene to the reference gene (HPRT) and the normalization of samples to the untreated control were calculated according to the $\Delta\Delta C_t$ method. The data represent the results of three independent experiments using cells from different donors.

Studies of peptide and LPS binding to human macrophages

Human macrophages were seeded in flow cytometry tubes at a density of 10^5 cells/tube. After adding peptides in PBS containing 2% FCS at the indicated concentrations, the cells were incubated at 4°C or 37°C for 5, 15, or 30 min. Subsequently, the cells were washed in ice-cold PBS with 2% FCS and azide (azide-PBS, 2% FCS), fixed in 2% paraformaldehyde for 15 min at room temperature, washed, and resuspended in 1 ml of azide-PBS, 2% FCS. For the fluorophore-quenching analysis, the samples were split, and one aliquot was pelleted by centrifugation and resuspended in 0.2% trypan blue in 0.75% NaCl directly prior to measurement. To study the effects of peptides on LPS binding, the macrophages were incubated with FITC-conjugated LPS in the presence or absence of peptides for 5, 15, or 30 min and subsequently washed and fixed. All samples were analyzed on a flow cytometer as described above. The data are representative of three to five independent experiments using cells from different donors.

588 **Confocal microscopic analysis of human macrophages**

589 Human macrophages were seeded in µ-Slides VI (Ibidi) at a density of 2×10^4 cells/well and
590 allowed to adhere for 24 h in an atmosphere of 37°C and 5% CO_2. LPS was labeled with
591 rhodamine-DHPE (Invitrogen) at a ratio of 10:1 (M) in chloroform/methanol and prepared as
592 described above. The cells were incubated with rhodamine-labeled LPS aggregates in the presence
593 of 1, 3, or 10 µM LL32 in PBS for 5 min at room temperature. Subsequently, the cells were washed
594 with PBS and fixed with 4% paraformaldehyde, and the nuclei were counterstained with Hoechst
595 (Invitrogen). The samples were analyzed using a Leica TCS SP5 confocal laser scanning
596 microscope (Leica Microsystems), and all images were acquired using Leica LAS AF software
597 with identical settings.

598

599 **Small-angle X-ray scattering (SAXS)**

600 X-ray scattering analyses of LPS in the presence and absence of peptides were performed using a
601 SAXS camera equipped with a linear position-sensitive detector (HECUS X-ray systems, Graz,
602 Austria). The camera was mounted on a sealed-tube X-ray generator (Seifert, Ahrensburg,
603 Germany), which was operated at 2 kW. CuKα radiation ($\lambda = 1.542$ Å) was selected using a Ni filter
604 and a pulse height discriminator. Silver stearate was used to perform the angular calibration of the
605 scattered intensities. LPS dispersions (50 mg/ml) or LPS:peptide mixtures (2:1 by weight) were
606 prepared in 20 mM HEPES (pH 7.0) as described for the preparation of aqueous dispersions of
607 LPS aggregates. The samples were measured using a thin-walled quartz capillary (diameter, 1 mm)
608 in a steel cuvette (Anton Paar, Graz, Austria) that had been inserted into a brass block. Automatic
609 temperature control was provided by a programmable Peltier unit. After a 10 min equilibration
610 period, scattering data for the small-angle region were recorded for each sample with an exposure
611 time of 1 h.

612 **Aggregate size and zeta potential measurements**

613 The size of LPS aggregates was measured by dynamic light scattering using a ZetaSizer Nano
614 device (Malvern Instruments) at 37°C. LPS aggregate preparations were diluted to 1 µM in 20 mM
615 HEPES, 150 mM NaCl, pH 7.4 and equilibrated for 3 min to 37°C. Peptides at 1 mM in 20 mM
616 HEPES, 150 mM NaCl, pH 7.4 were added consecutively to final concentrations of 1 – 100 µM.
617 After 3 min temperature equilibration the aggregate size was determined by triplicate
618 measurements. The data represent the means and ±SEM of ≥ 4 independent experiments performed
619 in triplicates. The Zeta potentials of LPS aggregates diluted to a final concentration of 2 µM in 20
620 mM HEPES (pH 7.0) were measured at 25°C. Peptides were added consecutively from a 2 or
621 20 µM stock solution in the same buffer to reach the indicated LPS to peptide molar ratio. The
622 velocity (v) of the LPS aggregates in a driving electric field with an effective voltage of 152 V was
623 measured via dynamic light scattering, and the corresponding electrophoretic mobilities (v/E) were
624 calculated. The associated Zeta potentials were calculated using the Smulochowski approximation.
625 The data represent the means and ±SEM of two independent experiments performed in triplicate.
626

627 **Analysis of the LBP–LPS interaction by ultracentrifugation**

628 The LBP–LPS interaction was studied using samples of LPS aggregates that had been incubated
629 with LBP in the absence or presence of peptides. LPS (4.55 µM) was incubated with recombinant
630 human LBP (XOMA Corp. Berkeley, CA, USA) at a molar ratio of 100:1 for 30 min at room
631 temperature in tubes that had been previously blocked for 1 h at 37°C with 10% BSA (w/v) in
632 20 mM HEPES. To investigate the effects of peptides, LL-32 and PMB were added to the LPS
633 aggregates at the indicated molar ratios before the addition of LBP. All LPS aggregates were
634 sedimented by ultracentrifugation at 117,000 g for 1 h at 4°C, and the supernatant and pellet
635 fractions were collected. The samples were separated using 12% SDS-PAGE and transferred to

nitrocellulose membranes for Western blotting. The membranes were incubated with an anti-LBP antibody (biG 42, 1:4000, Biometec, Greifswald, Germany) and goat anti-mouse IgG-HRP (1:10.000, Jackson ImmunoResearch) to detect bound LBP in the samples. The immunolabeled proteins were visualized using the ECL Plus Western blotting detection system (GE Healthcare). Band intensities were quantified using ImageJ 1.45S analysis software (US National Institutes of Health).

Confocal microscopic analysis of giant unilamellar vesicles (GUVs)

Giant unilamellar vesicles (GUVs) were prepared by electroformation as described elsewhere (60). Briefly, GUVs were reconstituted from 1,2-dioleoyl-sn-glycero-3-phosphocholine (DOPC), sphingomyelin (SM), and cholesterol (Chol) at a lipid ratio of 2:2:1 (M). Fluorescently labeled and biotinylated lipids were dissolved directly in ethanol (p.a.) to final concentrations of 0.5 and 2 mg/ml. Finally, GUVs were electroformed in 10 mM sucrose at 55°C for 5 h (3 V, 10 Hz) and cooled to room temperature overnight.

The supported biotinylated bilayer (SBB): DOPC was prepared by dissolution in $CHCl_3$ to a final concentration of 2 mg/ml and was mixed with biotinylated PE in a ratio of 99.5:0.5 mol%. The lipid mixture was evaporated under nitrogen, and the resulting lipid film was resolved in 5 mM HEPES (pH 7.4) to a final concentration of 1 mg/ml. Vesicles were formed by the application of ultrasound pulses (Ultrasonic-Homogenizer *HTU Soni130*, 2 min, pulse on/off: 2 s, amplitude 80%). The vesicle solution was pipetted directly into an eight-well microscopy chamber (LabTekII®, Thermo Fisher Scientific; 150 µl/well). Biotinylated vesicles were spread during overnight incubation at 4°C on a stirring plate (70 rpm).

Immobilization of GUVs (iGUVs) was achieved by linking the vesicles to the SBB using avidin–biotin chemistry. The GUVs were added to the SBB at a ratio of 3:1 (v/v) and linked by the addition

of 15 µl avidin (1 mg/ml in MilliQ), followed by a 30 min incubation. Fluorescence dye distribution was detected using a Leica TCS SP5 confocal laser scanning microscope (Leica Microsystems) equipped with Leica LAS AF software. For further processing, the user procedure *GUV-analysis.py* [Python(x, y), Version 2.7.6.1] was used to determine the fluorescent-dye-distribution-analysis (FDDA) of each channel. The program code will be provided upon request.

Atomic force microscopy

The aggregation of peptides on the solid-supported reconstituted membranes was investigated using an MPF3D atomic force microscope (Asylum Research). LPS, DOPC:SM:Chol, and PL_{MAK} membranes were prepared by allowing vesicles to spread on mica plates (1 cm^2) and were imaged in 2-3 ml of buffer at 23°C. The final LPS or lipid concentration was 25 µg/ml or 25 µM, respectively. The buffer, including any unbound LPS/lipids, was replaced prior to the addition of peptides at final concentrations of 25 µM during imaging. RC800PSA cantilevers (Olympus, Shinjuku, Japan; typical spring constant: $k \sim 0.1\ N \cdot m^{-1}$) or qp-BioAC (Nanosensors, Neuchatel, Switzerland; typical spring constant: $k \sim 0.1\ N \cdot m^{-1}$) were used in the AC mode. Images were processed in MFP-3D using IGOR Pro. DOPC:SM:Chol membranes were incubated in a buffer containing 100 mM NaCl, 50 mM HEPES, and 2 mM $CaCl_2$ (pH 7.4). Representative images out of at least three independent experiments are shown.

X-ray reflectivity (XRR) measurements

Solid supported membrane stacks of were prepared on silicon-(111)-wafers (dimensions of 10x15 mm^2) with a thickness of 500 µM (Silchem, Freiberg, Germany). Si-wafers were cleaned by subsequent and repeated sonication in MeOH and ultrapure water (three times, each step for 10 min). Right before sample deposition, wafers were plasma cleaned (air plasma, 2.5 min; PDC-

002, Harrick Plasma, Ithaca, NY, USA). DOPC:SM:Chol (2:2:1 M) dissolved in $CHCl_3$ (10 mg/mL) were either applied pure or mixed with LL-32 or PMB (4:1; v/v) on the Si-wafers. For full evaporation of the solvent, samples were dried overnight. Experiments were carried out at the synchrotron beamline P08 of PETRAIII (DESY, Hamburg) at a nominal humidity of 98% rH and a photon energy of 25 keV. The X-ray beam was collimated to a size of 150x500 µm² (v x h). Reflectivity profiles were acquired with an angular resolution of 0.01° and an acquisition time of 1 s for each position. XRR-data of solid supported membrane stacks were first evaluated with OriginPro® 8 (OriginLab Corporation, Northhampton, MA, USA) to obtain the electron density distribution. General proceedings include background and baseline corrections. Bragg peaks were fitted with a Gaussian or Lorentz fit.

Thermodynamic analysis

Thermodynamic effects of the binding of PMB to DOPC:SM:Chol liposome membranes were analyzed by differential scanning calorimetry. Calorimetry measurements were performed with a VP-DSC calorimeters (MicroCal, Inc., Northampton, MA, USA) at a heating and cooling rate of 1 $K \cdot min^{-1}$. The accuracy of the DSC experiments was $\Delta T = 0.1$ °C for the main phase transition temperatures. The measurements of DOPC:SM:Chol (9:9:2 M) small unilamellar liposomes at 10 mM in 20 mM HEPES, 150 mM NaCl, pH 7.4 were performed in the temperature interval from 5°C to 95°C. For each condition, five consecutive heating and cooling scans were performed to analyse the reproducibility of the DSC experiment. The DSC data were analysed using the Origin software. In the figure, only the temperature range at which phase transitions were observed is shown.

Surface acoustic wave (SAW) biosensor

Measurements were performed using functionalized gold-coated chips (S-sens K5 Biosensor Quartz Chips, SAW Instruments GmbH, Germany). Biomolecular interaction processes on the surface of the sensor chip can affect phase and amplitude of the surface guided acoustic wave. Changes of these parameters correlate with mass loading and viscosity changes on the chip surface. Following the immobilization of liposomes (500 µg ml^{-1} liposomes) on the positively ionized sensor chip surface, 100 µl of 25 µM solution of LL-32 or PMB were injected. Changes of phase and amplitude induced by the interaction of the peptides with the lipid bilayer were recorded over time. All biosensor measurements were performed at 22 °C. Averages of three independent experiments are given for each peptide.

Fluorescence polarization experiments

DOPC:SM:Chol (9:9:2 M) or PL_{MAK}:SM:Chol (2:0.5:0.5 M and 2:0.5:0.2 M) liposomes at 1mM in 20 mM HEPES, 150 mM NaCl, pH 7.4 were labeled at 0.5% (v/v) with 2 mM 1,6-diphenyl 1,3,5 hexatriene (DPH, Fluka, Seelze, Germany) in 96% ethanol directly before measurements. Before the measurements, the liposomes were diluted to 100 µM in 20 mM HEPES, 150 mM NaCl, pH 7.4 and experiments were performed as temperature scans between 15°C - 45°C at a heating rate of 1°C/min in a temperature controlled stirred cuvette of a Fluorolog SPEX (Jobin Yvon Inc., Edison, NJ, USA) to determine the temperature dependent membrane fluidity and phase transition of the membrane systems. Excitation light was polarized and emission analyzed parallel and perpendicular to the excitation light. Relative polarization of DPH emission was calculated according to the equation $P = (I_{\parallel} - I_{\perp})/(I_{\parallel} + I_{\perp})$. Buffer controls and peptide measurements were performed as independent measurements directly after the addition of the peptides at 25 µM final concentration.

For analysis of biological membranes, wild-type HEK293 cells were harvested, washed in PBS and suspended at $0.2*10^6$cells/mL in 20 mM HEPES, 150 mM NaCl, pH 7,4. Cells were maintained at 37°C, labeled with DPH at 0.05% (v/v) and directly analyzed for DPH-fluorescence polarization by fluorescence spectroscopy at constant temperature of 37°C in a cuvette with stirrer. Experiments were performed as time scans with 50 s of background measurement and subsequent addition of buffer, LL-32, or PMB at 25 µM final concentration. Data shown are control values at t = 50 s (control) and endpoint values after peptide addition t = 300 s.

Förster-Resonance Energy Transfer Assay

PL_{MAK}:SM:Chol (2:0.5:0.2 M) liposomes labeled with *NBD-PE (donor) and *Rh-DHPE (acceptor) in the chloroform phase at 100:1:1 molar ratio were diluted to 10 µM in 20 mM HEPES, 150 mM NaCl, pH 7.4. Measurements were performed at 37°C constant temperature on a Fluorolog-3 (Jobin Yvon Inc., Edison, NJ, USA). The fluorescence intensities I_{Donor} and $I_{Accceptor}$ were adjusted to equal intensities (ratio = 1) before the measurement and recorded for 50 s to obtain the baseline signal. Peptides were added to the liposomes at the indicated final concentrations and signals recorded for 50 s after each titration step. The ratios $I_{Donor}/I_{Acceptor}$ were calculated, with a ratio >1 indicating an increase and a ratio <1 indicating a decrease in membrane surface area.

Single-molecule fluorescence microscopy

TOCCSL ("Thinning Out Clusters while Conserving Stoichiometry of Labeling"), a single-molecule fluorescence modality (41, 61), was used to evaluate the mGFP-GPI homo-association on the plasma membranes of living CHO cells. Briefly, an Axiovert 200 microscope equipped with a 100x Plan-Apochromat objective (NA = 1.46; Zeiss) was used to illuminate samples in an objective-based total internal reflection (TIR) configuration via the epiport. Illumination at 488 nm

was provided by an Ar^+ laser (Model 2017-05AR, Spectra Physics) with a typical power of 2–11 kW/cm² on the sample. A slit aperture (Zeiss) with an approximate width of 7 µm in the object plane was used as a field stop to confine the area of illumination. To ensure exact timing, the excitation path was equipped with an acousto-optic modulator (Isomet) and a mechanical shutter (Vincent Associated). Timing protocols were generated using in-house programs implemented in Labview and were executed using a high-speed analog output card (National Instruments). The emission light was filtered (HQ535/50 and 505DCLP, Chroma), and fluorescence images were recorded using a back-illuminated, nitrogen-cooled CCD camera (ln/CCD-1340/1300-eb/1, Roper Scientific). To ensure precise temperature control, an in-house incubator equipped with a heating unit and an objective heater (PeCon) were used. All experiments were performed at 37°C.

After recording a pre-bleach image at a power density of 2 kW/cm² and an illumination time of 1 ms, the samples were bleached at a power density of 11 kW/cm² for 200–450 ms. The efficiency of photobleaching was tested by recording an image 1 ms after the bleach pulse. After a recovery period of 600–2400 ms, sequences of up to 10 images at a delay of 20 ms were recorded using the same illumination settings reported for the pre-bleach image. The first image after recovery was used to analyze the brightness of individual mGFP-GPI homo-associates, while the last image of the sequence was used to determine the reference brightness of a single mGFP molecule. Because only a small area of the cell was photobleached, multiple bleach- and recovery runs could be performed on a single cell.

For the analysis, single-molecule signals were analyzed using in-house algorithms implemented in MATLAB (MathWorks). The position, integrated brightness *B*, full width at half maximum, and local background of each signal was determined. The *B* values of single mGFP-GPI molecules were pooled from the final images of all TOCCSL sequences and used to calculate the probability density function (pdf) of the monomers as $\rho_1(B)$. The independent photon emission process

enabled the calculation of the corresponding pdfs of N co-localized emitters by a series of convolution integrals, $\rho_N(B) = \int \rho_1(B')\rho_{N-1}(B-B')dB'$. A weighted linear combination of these pdfs was then used to calculate the distribution of brightness in a mixed population of monomers and higher-order multimers, $\rho(B) = \sum_{N=1}^{N_{max}} \alpha_N \rho_N(B)$. The brightness values from all TOCCSL images of multiple cells per experimental condition were used to calculate $\rho(B)$. A least-square fit was applied to determine the weights of the individual pdfs, α_N, with $\sum_{N=1}^{N_{max}} \alpha_N = 1$. A minimum of 250–500 brightness values were used to calculate $\rho_1(B)$ and $\rho_N(B)$. To estimate the error bars, a random 50% subsample of the brightness values from all TOCCSL images was selected and used to calculate the fraction of homo-dimers, α_2. This sampling process was repeated 100 times, and the means and standard deviations (SD) of α_2 were calculated and are displayed as error bars. The statistical analysis was performed by comparing the single molecule brightness values of the peptide treatment and the control using a two-sample Kolmogorov-Smirnov test. Testing was done in Matlab using the implemented function kstest2.

Quantification and statistical analysis

The statistical analysis was performed using GraphPad Prism, versions 5 and 8 or Matlab. Details of the analyses are provided in the respective figure legends. A p-value ≤0.05 (*) was considered significant. No specific randomization method was used when handling samples or during experiments.

Materials Availability Statements

Data supporting the findings of this study are available from the authors upon reasonable request. The program code [Python(x, y), Version 2.7.6.1] of the fluorescent-dye-distribution-analysis (FDDA) of vesicles will be provided upon request.

Acknowledgements

We are grateful for the excellent technical assistance provided by Sabrina Groth, Irina von Cube, Christine Hamann, Kerstin Stephan, and our technician trainees. We are indebted to the Peptide Synthesis Core Facility for peptide synthesis. We thank the Bioanalytical Chemistry Group, Research Center Borstel for the mass spectrometry analysis of synthetic peptides. Confocal microscopy and flow cytometry were performed on instruments of the Flow Cytometry Core Unit of the Research Center Borstel. SAXS measurements were performed using the in-house radiation source at the Institute of Molecular Biosciences, University of Graz and the EMBL beamlines P08 and P12, DESY, Hamburg (beamtime granted to A.B.S., K.B., T.G). This project was supported by the Deutsche Forschungsgemeinschaft (DFG, German Research Foundation), Cluster of Excellence 306/2 “Inflammation at Interfaces” (Excellence Initiative, Germany, since 2006, DFG-Project No. 49701054), grant Exc306 RA3 to A.B.S. and T.G..” GMT was funded by grants from Proyectos de Investigación Universidad de Navarra (PIUNA-P2011-17 and P2015-14) and by a grant from Ministerio de Sanidad y Consumo (FIS-PI050768), Spain.

REFERENCES

1. M. A. Kovach, *et al.*, Cathelicidin-related antimicrobial peptide is required for effective lung mucosal immunity in Gram-negative bacterial pneumonia. *J. Immunol.* **189**, 304-311 (2012).
2. B. J. McHugh, *et al.*, Cathelicidin is a "fire alarm", generating protective NLRP3-dependent airway epithelial cell inflammatory responses during infection with Pseudomonas aeruginosa. *PLoS pathog.* **15**, e1007694 (2019).
3. L. J. Zhang, *et al.*, Age-Related Loss of Innate Immune Antimicrobial Function of Dermal Fat Is Mediated by Transforming Growth Factor Beta. *Immunity* **50**, 121-136 e125 (2019).
4. WHO, Antimicrobial resistance: global report on surveillance 2014. pp. 1-232 (2014).
5. U.S. Department of Health and Human Services (2013) *Antibiotic resistance threats in the United States, 2013* (U.S. Department of Health and Human Services, Centers for Disease Control and Prevention, 2013), pp. 1-114..
6. B. P. Lazzaro, M. Zasloff, & J. Rolff, Antimicrobial peptides: Application informed by evolution. *Science* **368**, (6490):eaau5480. (2020).
7. R. E. Hancock, A. Nijnik, & D. J. Philpott, Modulating immunity as a therapy for bacterial infections. *Nat. Rev. Microbiol.* **10**, 243-254 (2012).
8. S. C. Mansour, O. M. Pena, & R. E. Hancock, Host defense peptides: front-line immunomodulators. *Trends Immunol.* **35**, 443-450 (2014).
9. R. E. Hancock, E. F. Haney, & E. E. Gill, The immunology of host defence peptides: beyond antimicrobial activity. *Nat. Rev. Immunol.* **16**, 321-334 (2016).
10. J. Cohen, The immunopathogenesis of sepsis. *Nature* **420**, 885-891 (2002).
11. E. F. Haney, S. K. Straus, & R. E. W. Hancock, Reassessing the Host Defense Peptide Landscape. *Front. Chem.* **7**, 43 (2019).
12. J. Wehkamp, *et al.*, Reduced Paneth cell alpha-defensins in ileal Crohn's disease. *Proc. Nat. Acad. Sci. U.S.A* **102**, 18129-18134 (2005).
13. J. Turner, Y. Cho, N. N. Dinh, A. J. Waring, & R. I. Lehrer, Activities of LL-37, a cathelin-associated antimicrobial peptide of human neutrophils. *Antimic. Agents Chemother.* **42**, 2206-2214 (1998).
14. C. Beisswenger, *et al.*, Allergic airway inflammation inhibits pulmonary antibacterial host defense. *J. Immunol.* **177**, 1833-1837 (2006).
15. P. S. Hiemstra, G. D. Amatngalim, A. M. van der Does, & C. Taube, Antimicrobial Peptides and Innate Lung Defenses: Role in Infectious and Noninfectious Lung Diseases and Therapeutic Applications. *Chest* **149**, 545-551 (2016).
16. K. Lohner, Membrane-active Antimicrobial Peptides as Template Structures for Novel Antibiotic Agents. *Curr. Topics Med. Chem.* **17**, 508-519 (2017).
17. K. Lohner & S. E. Blondelle, Molecular mechanisms of membrane perturbation by antimicrobial peptides and the use of biophysical studies in the design of novel peptide antibiotics. *Comb. Chem. High Throug. Screen.* **8**, 241-256 (2005).
18. R. E. Hancock & H. G. Sahl, Antimicrobial and host-defense peptides as new anti-infective therapeutic strategies. *Nat. Biotechnol.* **24**, 1551-1557 (2006).
19. Y. De, *et al.*, LL-37, the neutrophil granule- and epithelial cell-derived cathelicidin, utilizes formyl peptide receptor-like 1 (FPRL1) as a receptor to chemoattract human peripheral blood neutrophils, monocytes, and T cells. *J. Exp. Med.* **192**, 1069-1074 (2000).
20. D. M. E. Bowdish, D. J. Davidson, D. P. Speert, & R. E. W. Hancock, The Human Cationic Peptide LL-37 Induces Activation of the Extracellular Signal-Regulated Kinase and p38 Kinase Pathways in Primary Human Monocytes. *J. Immunol.* **172**, 3758-3765 (2004).
21. N. Mookherjee, *et al.*, Intracellular receptor for human host defense peptide LL-37 in monocytes. *J. Immunol.* **183**, 2688-2696 (2009).
22. L. Heinbockel, *et al.*, Preclinical investigations reveal the broad-spectrum neutralizing activity of peptide Pep19-2.5 on bacterial pathogenicity factors. *Antimicrob. Agents Chemother.* **57**, 7 (2013).

23. M. M. Domingues, *et al.*, Biophysical characterization of polymyxin B interaction with LPS aggregates and membrane model systems. *Biopolymers* **98**, 338-344 (2012).
24. B. Beutler & E. T. Rietschel, Innate immune sensing and its roots: The story of endotoxin. *Nat. Rev. Immunol.* **3**, 169-176 (2003).
25. A. Poltorak, *et al.*, Defective LPS signaling in C3H/HeJ and C57BL/10ScCr mice: mutations in Tlr4 gene. *Science* **282**, 2085-2088 (1998).
26. K. Hoshino, *et al.*, Cutting edge: Toll-like receptor 4 (TLR4)-deficient mice are hyporesponsive to lipopolysaccharide: evidence for TLR4 as the Lps gene product. *J. Immunol.* **162**, 3749-3752 (1999).
27. R. Shimazu, *et al.*, MD-2, a molecule that confers lipopolysaccharide responsiveness on Toll-like receptor 4. *J. Exp. Med.* **189**, 1777-1782 (1999).
28. A. B. Schromm, *et al.*, Molecular genetic analysis of an endotoxin nonresponder mutant cell line: a point mutation in a conserved region of MD-2 abolishes endotoxin-induced signaling. *J. Exp. Med.* **194**, 79-88 (2001).
29. N. J. Gay, M. F. Symmons, M. Gangloff, & C. E. Bryant, Assembly and localization of Toll-like receptor signalling complexes. *Nat. Rev. Immunol.* **14**, 546-558 (2014).
30. R. R. Schumann, *et al.*, Structure and function of lipopolysaccharide binding protein. *Science* **249**, 1429-1431 (1990).
31. S. D. Wright, R. A. Ramos, P. S. Tobias, R. J. Ulevitch, & J. C. Mathison, CD14, a receptor for complexes of lipopolysaccharide (LPS) and LPS binding protein. *Science* **249**, 1431-1433 (1990).
32. T. L. Gioannini, *et al.*, Isolation of an endotoxin-MD-2 complex that produces Toll-like receptor 4-dependent cell activation at picomolar concentrations. *Proc. Nat. Acad. Sci. U.S.A.* **101**, 4186-4191 (2004).
33. T. Gutsmann, *et al.*, New antiseptic peptides to protect against endotoxin-mediated shock. *Antimicrob. Agents Chemother.* **54**, 3817-3824 (2010).
34. D. S. Uppu & J. Haldar, Lipopolysaccharide Neutralization by Cationic-Amphiphilic Polymers through Pseudoaggregate Formation. *Biomacromolecules* **17**, 862-873 (2016).
35. J. Andrä, T. Gutsmann, P. Garidel, & K. Brandenburg, Mechanisms of endotoxin neutralization by synthetic cationic compounds. *J. Endotox. Res.* **12**, 261-277 (2006).
36. V. A. K. Rathinam, Y. Zhao, & F. Shao, Innate immunity to intracellular LPS. *Nat. Immunol.* **20**, 527-533 (2019).
37. A. B. Schromm, *et al.*, The charge of endotoxin molecules influences their conformation and IL-6-inducing capacity. *J. Immunol.* **161**, 5464-5471 (1998).
38. P. Garidel, *et al.*, Divalent cations affect chain mobility and aggregate structure of lipopolysaccharide from Salmonella minnesota reflected in a decrease of its biological activity. *Biochim. Biophys. Acta* **1715**, 122-131 (2005).
39. M. Triantafilou, K. Miyake, D. T. Golenbock, & K. Triantafilou, Mediators of innate immune recognition of bacteria concentrate in lipid rafts and facilitate lipopolysaccharide-induced cell activation. *J. Cell Sci.* **115,** 2603-2611 (2002).
40. M. Triantafilou, S. Morath, A. Mackie, T. Hartung, & K. Triantafilou, Lateral diffusion of Toll-like receptors reveals that they are transiently confined within lipid rafts on the plasma membrane. *J. Cell Sci.* **117**, 4007-4014 (2004).
41. M. Brameshuber, *et al.*, Imaging of mobile long-lived nanoplatforms in the live cell plasma membrane. *J. Biol. Chem.* **285**, 41765-41771 (2010).
42. S. Saitoh, *et al.*, Lipid A antagonist, lipid IVa, is distinct from lipid A in interaction with Toll-like receptor 4 (TLR4)-MD-2 and ligand-induced TLR4 oligomerization. *Internat. Immunol.* **16**, 961-969 (2004).
43. B. S. Park, *et al.*, The structural basis of lipopolysaccharide recognition by the TLR4-MD-2 complex. *Nature* **458**, 1191-1195 (2009).
44. P. G. Motshwene, *et al.*, An oligomeric signaling platform formed by the Toll-like receptor signal transducers MyD88 and IRAK-4. *J. Biol. Chem.* **284**, 25404-25411 (2009).
45. Y. Sun, *et al.*, Free cholesterol accumulation in macrophage membranes activates Toll-like receptors and p38 mitogen-activated protein kinase and induces cathepsin K. *Circ. Res.* **104**, 455-465 (2009).

46. M. B. Fessler & J. S. Parks, Intracellular lipid flux and membrane microdomains as organizing principles in inflammatory cell signaling. *J. Immunol.* **187**, 1529-1535 (2011).
47. A. L. Hilchie, K. Wuerth, & R. E. Hancock, Immune modulation by multifaceted cationic host defense peptides. *Nat. Chem. Biol.* **9**, 761-768 (2013).
48. F. D. Oakley, R. L. Smith, & J. F. Engelhardt, Lipid rafts and caveolin-1 coordinate interleukin-1beta (IL-1beta)-dependent activation of NFkappaB by controlling endocytosis of Nox2 and IL-1beta receptor 1 from the plasma membrane. *J. Biol. Chem.* **284**, 33255-33264 (2009).
49. J. E. S. Doan, D. A. Windmiller, & D. W. H. Riches, Differential Regulation of TNF-R1 Signaling: Lipid Raft Dependency of p42mapk/erk2 Activation, but Not NF-κB Activation. *J. Immunol.* **172**, 7654-7660 (2004).
50. N. Mookherjee, *et al.*, Modulation of the TLR-Mediated Inflammatory Response by the Endogenous Human Host Defense Peptide LL-37. *J. Immunol.* **176**, 2455-2464 (2006).
51. J. Yu, *et al.*, Host Defense Peptide LL-37, in Synergy with Inflammatory Mediator IL-1 , Augments Immune Responses by Multiple Pathways. *J. Immunol.* **179**, 7684-7691 (2007).
52. E. Lopez-Collazo & C. del Fresno, Pathophysiology of endotoxin tolerance: mechanisms and clinical consequences. *Crit. Care* **17**, 242 (2013).
53. T. van der Poll, F. L. van de Veerdonk, B. P. Scicluna, & M. G. Netea, The immunopathology of sepsis and potential therapeutic targets. *Nat. Rev. Immunol.* **17**, 407-420 (2017).
54. A. Boto, J. M. Perez de la Lastra, & C. C. Gonzalez, The Road from Host-Defense Peptides to a New Generation of Antimicrobial Drugs. *Molecules* **23**, 311 (2018).
55. A. Luther, *et al.*, Chimeric peptidomimetic antibiotics against Gram-negative bacteria. *Nature* **576,** 452-458 (2019).
56. W. Brabetz, S. Muller-Loennies, O. Holst, & H. Brade, Deletion of the heptosyltransferase genes rfaC and rfaF in Escherichia coli K-12 results in an Re-type lipopolysaccharide with a high degree of 2-aminoethanol phosphate substitution. *Eur. J. Biochem. / FEBS* **247**, 716-724 (1997).
57. C. Galanos, O. Lüderitz, & O. Westphal, A new method for the extraction of R lipopolysaccharides. *Eur. J. Biochem. / FEBS* **9**, 245-249 (1969).
58. C. Galanos, M. A. Freudenberg, & W. Reutter, Galactosamine-induced sensitization to the lethal effects of endotoxin. *Proc. Nat. Acad. Sci. U.S.A.* **76**, 5939-5943 (1979).
59. S. P. Keese, K. Brandenburg, M. Roessle, & A. B. Schromm, Pulmonary surfactant protein A-induced changes in the molecular conformation of bacterial deep-rough LPS lead to reduced activity on human macrophages. *Innate Immunity* **20**, 787-798 (2014).
60. S. L. Veatch, Electro-formation and fluorescence microscopy of giant vesicles with coexisting liquid phases. *Methods Mol. Biol.* **398**, 59-72 (2007).
61. M. Moertelmaier, M. Brameshuber, M. Linimeier, G. J. Schütz, & H. Stockinger, Thinning out clusters while conserving stoichiometry of labeling. *Appl. Phys. Lett.* **87**, 263903 (2005).

809

FIGURE LEGENDS

Figure 1: Antimicrobial peptides (AMPs) and PMB inhibit lipopolysaccharide (LPS)-mediated inflammation *in vitro* and *in vivo*

(**a**) AMPs and PMB inhibit LPS-induced TNF-α production in macrophages. Human macrophages were incubated in medium alone or in the presence of 0.1, 1, 3, 10, and 20 µM concentrations of the peptides LL-32, NK-2, Pep19-2.5, hBD-3-l, or PMB for 30 min at 37°C. The macrophages were subsequently stimulated with 5 nM LPS for 4 h at 37°C. The concentrations of TNF-α in the supernatants were determined. TNFα values of samples stimulated with LPS in the absence of peptide were set 100% and all other values were calculated accordingly. The data are shown as the means ± standard errors of the means (SEM) of n = 8 (LL-32), n = 4-5 (NK-2, Pep19-2.5, hBD-3-l), or n = 5-9 (PMB) independent experiments using cells from different donors.

(**b**) LL-32 and PMB-mediated rescue from lethal LPS-induced sepsis. Galactosamine-sensitized mice were injected intraperitoneally with LPS (100 ng/mouse; equivalent to 5 µg/kg) and subsequently with 50 or 100 µg/mouse of LL-32 or PMB or saline (n = 8 mice per group) at a different injection site. The survival of the mice was monitored daily.

(**c**) The biological effects of LL-32 and PMB on human macrophages are resistant to washing. Macrophages were incubated with 10 µM LL-32 or PMB for 30 min at 37°C and subsequently washed three times with serum-free RPMI medium to remove unbound peptide or left untreated, followed by stimulation with 5 nM LPS for 4 h. The concentrations of TNF-α in the supernatants were determined. TNFα values of samples stimulated with LPS in the absence of peptide were set 100% and all other values were calculated accordingly. The data are shown as the means ± SEM of n = 3 independent experiments using cells from different donors. Black dots represent the individual data points. Control, unstimulated cells; n.d., not detectable.

834 Statistical analyses were performed via one-way ANOVA and Dunnett's post test; *$p \leq 0.05$,
835 **$p \leq 0.01$, and ***$p \leq 0.001$ (peptide groups versus LPS control).
836
837 **Figure 2: LL-32 and PMB binding modifies cellular lipopolysaccharide (LPS) processing and**
838 **inhibits inflammatory responses in human macrophages**
839 (**a**) Macrophages were incubated with LL-32-NBD, Pep19-2.5-NBD, or PMB-BODIPY for 5 min
840 at 37°C, and then washed and fixed. Subsequently, the samples were split and analyzed by flow
841 cytometry to determine the total bound peptide directly and after quenching with 0.2% trypan blue
842 to determine the amount of intracellular peptide.
843 (**b**) Macrophages were incubated with 3 µM LPS-FITC in the presence of 3 µM LL-32 for 5, 15 or
844 30 min at 37°C. The samples were analyzed by flow cytometry.
845 (**c**) Macrophages cultured on µ-slides were stimulated with rhodamine-labeled LPS in the presence
846 of 1, 3, and 10 µM LL-32 for 5 min at room temperature. Cell nuclei were counterstained with
847 Hoechst. The scale bar represents 25 µM.
848 (**d**) Macrophages were preincubated for 30 min with LL-32 (1, 3, and 10 µM) or PMB (1 µg/ml,
849 0.84 µM) and stimulated with 5 nM LPS for 1 h at 37°C. Gene expression was analyzed by qRT-
850 PCR. Data are presented as the relative expression ratios of the target to reference gene (HPRT),
851 normalized to the untreated control.
852 **e**) Macrophages were preincubated with LL-32 (3 and 10 µM), PMB (1 µg/ml, 0.84 µM), or buffer
853 (control) for 30 min at 37°C and subsequently stimulated with LPS for 4 h in the presence of
854 10 µg/ml bafilomycin to prevent cytokine secretion. Intracellular TNF-α was stained with a
855 specific antibody, and the cells were analyzed by flow cytometry. Numbers in the upper right
856 quadrants of plots indicate the percentages of gated macrophages positive for TNF-α. Data are
857 representative of n = 3 (a, c, d, e) and n = 5 (b) independent experiments.

Figure 3: LL-32 and PMB affect the supramolecular organization and binding interactions of lipopolysaccharide (LPS)

(**a**) The size of LPS aggregates was determined by dynamic light scattering experiments of LPS aggregates at 1 µM concentration in 20 mM HEPES, 150 mM NaCl, pH 7.4 at 37°C. Buffer (volume control) or peptides were added at the indicated final concentrations, samples equilibrated for 3 min, and aggregate size determined by triplicate measurements. The data represent the means ± SEM of n=4 (buffer control), n=7 (LL-32), and n=5 (PMB) independent experiments. Data were analyzed as peptide versus control by One-way ANOVA with Dunnett`s post-test. **$p \leq 0.01$ and ***$p \leq 0.001$; n.s., not significant.

(**b**) Zeta potentials of LPS aggregates in solution. LL-32 and PMB were titrated to LPS at the indicated molar ratios. The data represent the means ± SEM of two independent experiments with three technical replicates.

(**c**) Atomic force microscopy (AFM) images and height profiles of solid-supported layers of LPS WBB01. Pure LPS was immobilized as the control (upper graph) or preincubated with LL-32 (middle graph) or PMB (lower graph) at a ratio of 2:1 (by weight). Data are representative of n = 3 independent experiments.

(**d**) Small-angle X-ray scattering (SAXS) diffractograms of pure LPS aggregates (top panel) and aggregates prepared in the presence of LL-32 (middle panel) or PMB (bottom panel) at a LPS:peptide ratio of 2:1 (by weight). The diffractograms are representative of n = 3 independent experiments.

(**e**) LPS (4.55 µM) and LBP (500 ng) were co-incubated with LL-32 or PMB in 200 µl of 20 mM HEPES (pH 7.0) at the indicated molar ratios for 30 min at room temperature, and subsequently sedimented via ultracentrifugation at 117,000 × g. Supernatant (S) and pellet (P) fractions were separated by SDS-PAGE and immunoblotted to detect LBP. Representative images

of the blots of LL-32 (upper panel) and PMB (lower panel) from n = 4 independent experiments each are shown.

(**f**) Quantification of the band intensities of the pellet fractions. The data were quantified using Image J software, and the pixel intensities of the pellet fractions of four independent experiments were normalized to the control sample (LBP + LPS). The statistical analyses were performed using a one-way ANOVA and Dunnett's post test. The graph presents the means ± SEM of n = 4 independent experiments; **$p \leq 0.01$ and ***$p \leq 0.001$ (LPS only versus LPS + peptide).

Figure 4: The anti-inflammatory effects of LL-32 and PMB are mediated by peptide–cell interactions

(**a**) HEK293-TLR4/MD-2 cells in DMEM containing 10% fetal calf serum (FCS) were seeded into plates at a density of 5×10^5/well and treated with LL-32 or PMB at the indicated concentrations for 30 min at 37°C. The cells were washed three times in DMEM to remove peptides from the medium and were subsequently stimulated with 10 nM lipopolysaccharide (LPS) for 24 h.

(**b**) HEK293-TLR4/MD-2 cells were treated with LL-32 or PMB for 30 min at 37°C, followed directly by stimulation with 10 nM LPS for 24 h.

(**c**) HEK293-TLR4/MD-2 cells were treated with LL-32 or PMB for 30 min at 37°C, followed directly by stimulation with 100 nM IL-1β or (**d**) 50 nM TNF-α. The concentrations of secreted IL-8 in the supernatants were determined by ELISA. IL-8 values of cells stimulated with LPS in the absence of peptide were set 100% and all other values were calculated accordingly. The data are reported as the means and ± SEM of n = 3 (a), n = 8-13 (b), n = 7 (c), and n = 5 (d) independent experiments. White dots represent the individual data points.

(**e**) Cholesterol-dependent downregulation of the LPS response. HEK293-TLR4/MD-2 cells in DMEM containing 1% FCS were seeded as described in (**a)** and treated with 0.05 – 5 mM

906 *β*-methyl-cyclodextrin (ß-CD) for 60 min at 37°C, washed with DMEM containing 10% FCS, and
907 stimulated with 50 nM LPS for 24 h. The concentrations of IL-8 in the supernatants were
908 determined by ELISA. IL-8 values of samples stimulated with LPS without ß-CD treatment were
909 set 100%. Data are shown as the means and ± SEM of n = 7 independent experiments. White dots
910 represent the individual data points.
911 The statistical analyses (a–e) were performed using one-way ANOVA and Dunnett's post test;
912 *$p \leq 0.05$, **$p \leq 0.01$, ***$p \leq 0.001$, and ****$p \leq 0.0001$ (peptide groups versus LPS control).
913
914 **Figure 5: LL-32 and PMB interact via opposing interaction sites on cholesterol-rich model**
915 **membranes**
916 (**a**) False-color presentation of the distributions of LL-32-Rho and BODIPY-PMB on immobilized
917 giant vesicles reconstituted from the DOPC:SM:Chol raft-mixture (2:2:1 M). The membrane was
918 labeled using the lipid-dye conjugate BODIPY-PC (upper panel) or Atto633-DOPE (lower panel).
919 The l_d domain is shown in cyan, and cholesterol-rich (l_o-) domains appear black. After incubation
920 with either 4.5 µM LL-32-Rho or 22.5 µM BODIPY-PMB (magenta), the prevalence of each
921 peptide could be estimated by a fluorescent-dye-distribution-analysis (FDDA) to determine the
922 correlation or anti-correlation of the two dyes. Scale bars represent 10 µm. The experiments were
923 performed in 5 mM HEPES (pH 7.4) at 23°C. The data are representative of n = 3 independent
924 experiments.
925 (**b**) Atomic force microscopy (AFM) images and height histograms of the solid-supported bilayers
926 of DOPC:SM:Chol (9:9:2 M). DOPC:SM:Chol bilayers were immobilized on mica and washed.
927 Peptides were added to a final concentration of 25 µM. The presented images were obtained before
928 and 30 minutes after the addition of peptide (or buffer as a control). The data are representative of
929 n = 3 independent experiments.

(**c**) AFM images of solid-supported bilayers of the macrophage mimetic lipid mixture PL_{MAK}:SM:Chol (2:0.5:0.2 M). Bilayers were immobilized on mica in 20 mM HEPES, 150 mM NaCl, pH 7.4 containing 1 mM $MgCl_2$ and peptides were added to a final concentration of 25 µM. The presented images were obtained before and after the addition of peptide or buffer at the indicated times. The data are representative of n = X (LL-32) and n = Y (PMB) independent experiments.

Figure 6: LL-32 and PMB differentially interact with complex eukaryotic membranes and influence the homo-association of GPI-anchored proteins in the exoplasmic leaflet of the plasma membrane

(**a**) Binding of peptides to immobilized PL_{MAK}:SM:Chol (2:0.5:0.2 M) membranes was determined by surface acoustic wave (SAW) measurements on a S-sens K5 Biosensor. The graph presents the means ± SEM of n = 3 independent experiments.

(**b**) Changes in the membrane surface area were analyzed by a Förster-resonance energy-transfer (FRET)-based assay. PL_{MAK}:SM:Chol (2:0.5:0.2 M) liposomes containing *NBD-PE (donor) and *Rh-DHPE (acceptor) as membrane labels were diluted to 10 µM in 20 mM HEPES, 150 mM NaCl, pH 7.4. The fluorescence intensities I_{donor} and $I_{acceptor}$ were recorded for 50 s to obtain the baseline signal. Peptides were added to the liposomes at the indicated final concentrations and signals recorded for 50 s after each titration step. Ratios $I_{Donor}/I_{Acceptor}$ were calculated. Data represent the means of n = 3 independent measurements.

(**c**) Ratios $I_{Donor}/I_{Acceptor}$ after LL-32 and PMB titration from experiments displayed in (**b**) on PL_{MAK}:SM:Chol (2:0.5:0.2 M) liposomes. Data are values at 50 s after addition of peptides at the indicated concentrations and display means ± SEM of n = 3 independent experiments. Data were

analyzed by two-tailed t-test of paired samples (peptide versus control); ***$p \leq 0.001$, n.s. not significant.

(**d**) Liposome membranes of DOPC:SM:Chol (9:9:2 M) or PL_{MAK}:SM:Chol (2:0.5:0.5 and 2:0,5:0,2 M) were labeled with DPH and membrane fluidity was determined as relative polarization of the fluorescence emission of DPH. Measurements were performed as temperature scans from 15 - 45°C. Peptides were added to a final concentration of 25 µM and the temperature scan was started immediately. Data depicted are representative of n = 3-4 independent experiments.

(**e**) Relative polarization data of (**d**) at the physiological temperature 37°C. Data are mean and SEM of n = 3-4 independent experiments. Data were analyzed by two-tailed t-test of unpaired samples (peptide or buffer versus control); ***$p \leq 0.001$, n.s. not significant.

(**f**) HEK293 wildtype cells were labeled with DPH and measured at $0.2*10^6$ cells/ml at 37°C constant temperature. Baseline signal was recorded for 50 sec, then peptides were added to a final concentration of 25 µM and signals recorded until 300 sec. Data are means and SEM at t= 50 sec (C) and t = 300 sec (+ buffer/peptide) of n=5 independent experiments. Data were analyzed by two-tailed t-test of paired samples (peptide or buffer versus control); ****$p \leq 0.0001$, n.s. not significant.

(**g**) Single-molecule TOCCSL experiments were performed to determine the degree of mGFP-GPI homo-association in the plasma membranes of living CHO cells. The addition of both the LL-32 and PMB peptides caused a substantial change in mGFP-GPI homo-association, as demonstrated by an increase (LL-32, n = 10 cells) and decrease (PMB, n = 8 cells) in the mGFP-GPI dimer fraction. Data are shown as the mean and ± SEM. Statistical analysis was performed using a two-sample Kolmogorov-Smirnov test; ****$p \leq 0.0001$ (peptide versus control).

977 **Figure 7: Model of the modes of AMP function.**

978 (**a**) AMPs have different levels of interaction that lead to the neutralization of inflammatory cell
979 activation by lipopolysaccharide (LPS): 1. direct interaction with LPS, leading to biophysical
980 changes and a biologically less active LPS structure; 2. interference with the interaction between
981 LPS and transport proteins in serum (i.e., LPS-binding protein, soluble CD14) or cellular LPS
982 receptor proteins (membrane-bound CD14 and TLR4/MD-2 receptor); and 3. reorganization of
983 cholesterol-containing membrane domains. Enlargement box of the host cell cytoplasmic
984 membrane depicts the differential mechanisms of membrane interaction as observed for LL-32 (left
985 panel; step I model is based on the experimental data, step II model is the suggested most likely
986 biophysical model to explain the data) and PMB (right panel) membrane interaction.

Figure 1

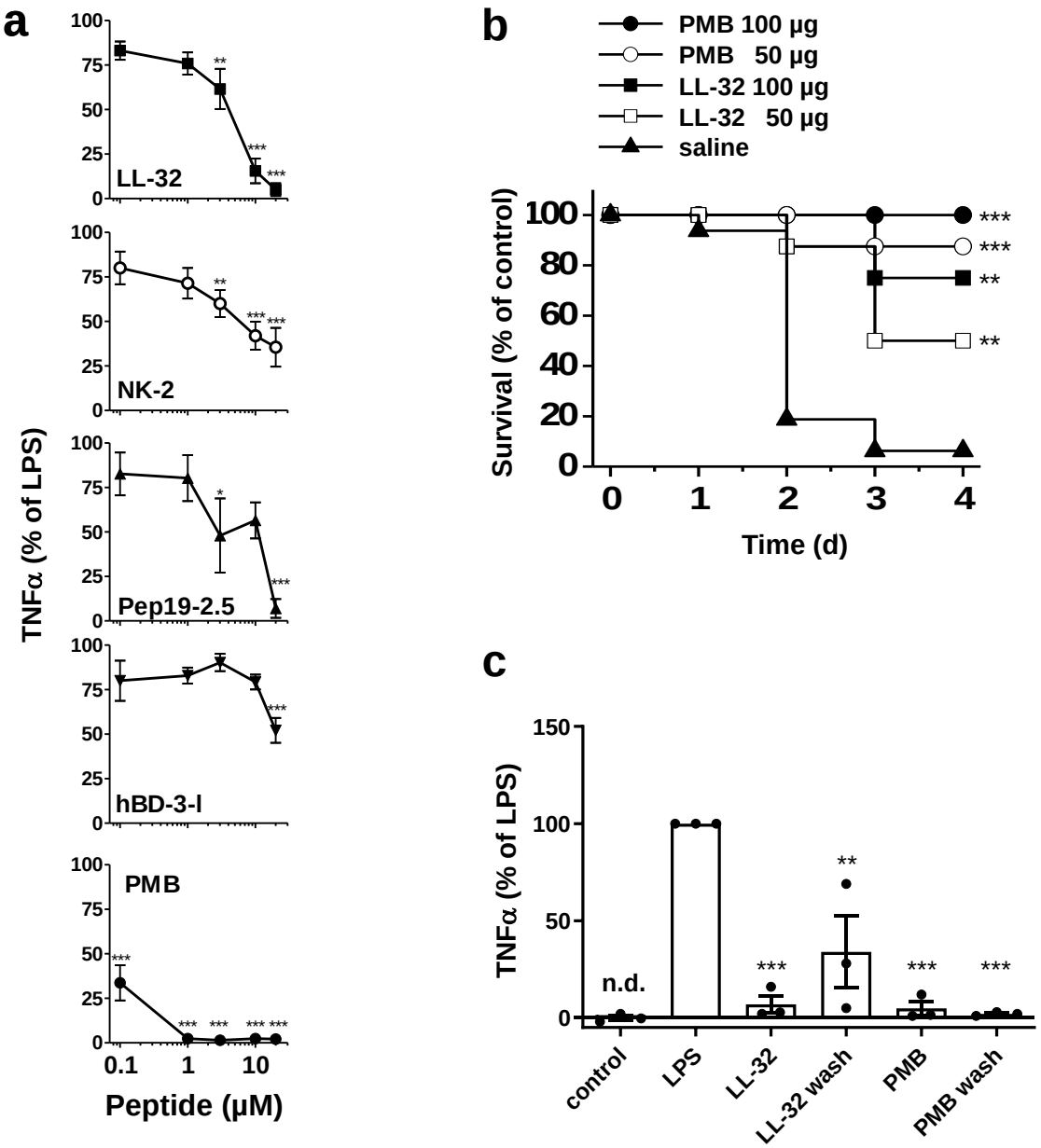
a
TNFα (% of LPS)
LL-32
NK-2
Pep19-2.5
hBD-3-l
PMB
Peptide (μM)
b
PMB 100 μg
PMB 50 μg
LL-32 100 μg
LL-32 50 μg
saline
Survival (% of control)
Time (d)
c
TNFα (% of LPS)
n.d.
control
LPS
LL-32
LL-32 wash
PMB
PMB wash

Figure 2

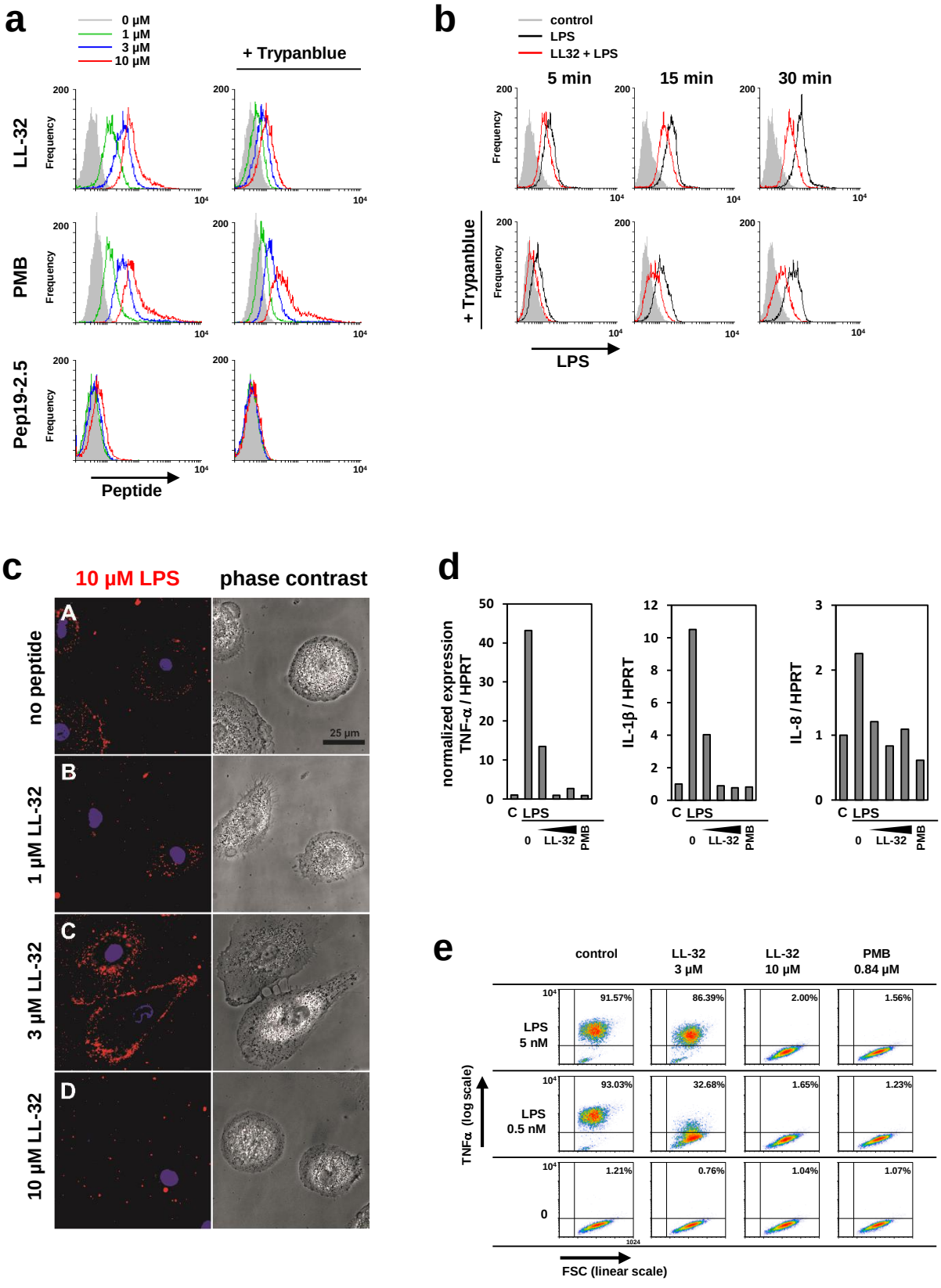
a
0 µM
1 µM
3 µM
10 µM
+ Trypanblue
LL-32
PMB
Pep19-2.5
Frequency
Peptide
b
control
LPS
LL32 + LPS
5 min
15 min
30 min
+ Trypanblue
LPS
c
10 µM LPS
phase contrast
no peptide
1 µM LL-32
3 µM LL-32
10 µM LL-32
25 µm
d
normalized expression
TNF-α / HPRT
IL-1β / HPRT
IL-8 / HPRT
C LPS
0 LL-32 PMB
e
control
LL-32 3 µM
LL-32 10 µM
PMB 0.84 µM
LPS 5 nM
LPS 0.5 nM
91.57%
86.39%
2.00%
1.56%
93.03%
32.68%
1.65%
1.23%
1.21%
0.76%
1.04%
1.07%
TNFα (log scale)
FSC (linear scale)

Figure 3

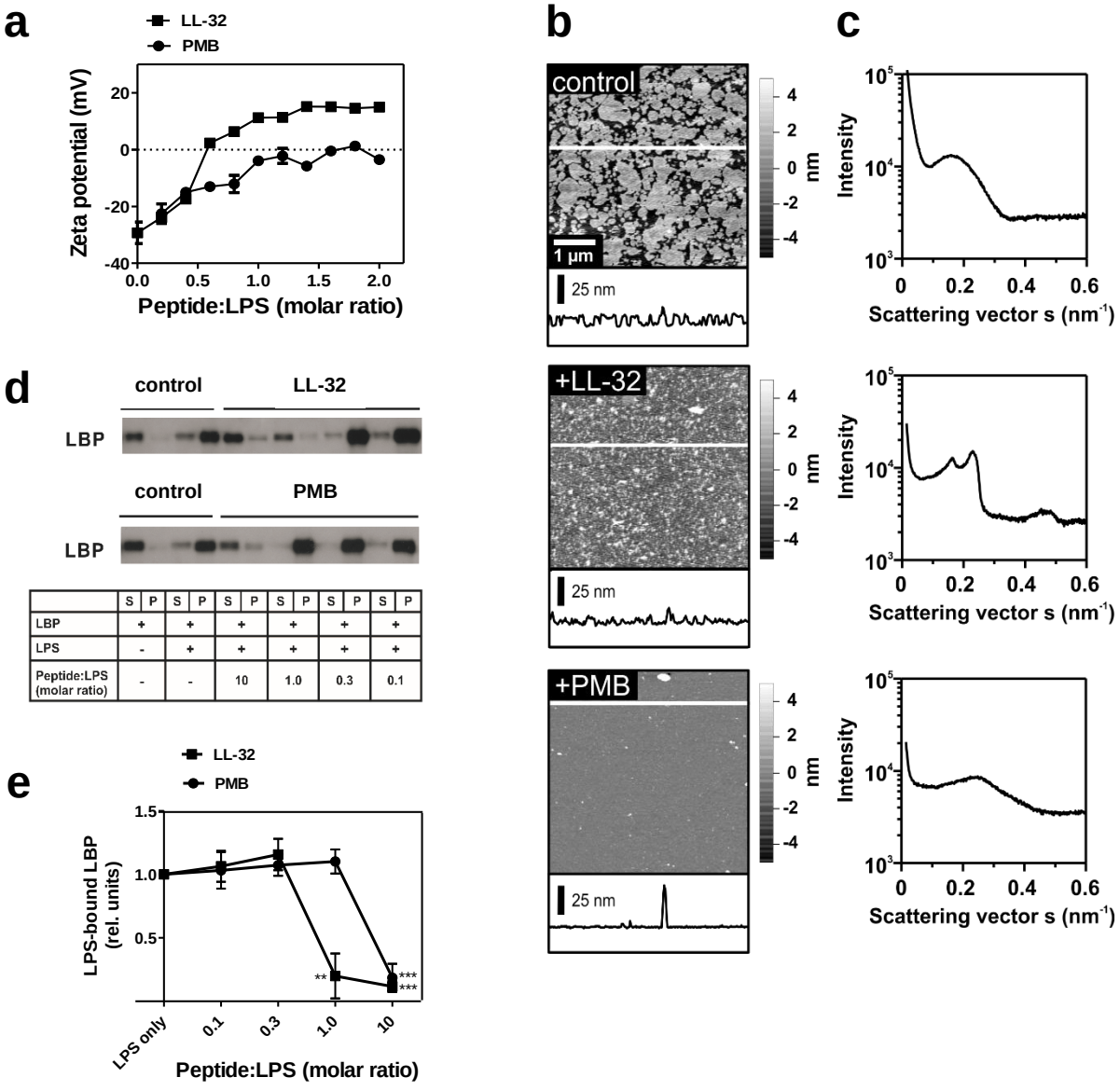
a
LL-32
PMB
Zeta potential (mV)
Peptide:LPS (molar ratio)
b
control
1 µm
25 nm
+LL-32
+PMB
nm
c
Intensity
Scattering vector s (nm-1)
d
control
LL-32
LBP
control
PMB
LBP
S P S P S P S P S P S P
LBP + + + + + +
LPS - + + + + +
Peptide:LPS (molar ratio) - - 10 1.0 0.3 0.1
e
LL-32
PMB
LPS-bound LBP (rel. units)
LPS only
0.1
0.3
1.0
10
Peptide:LPS (molar ratio)

Figure 4

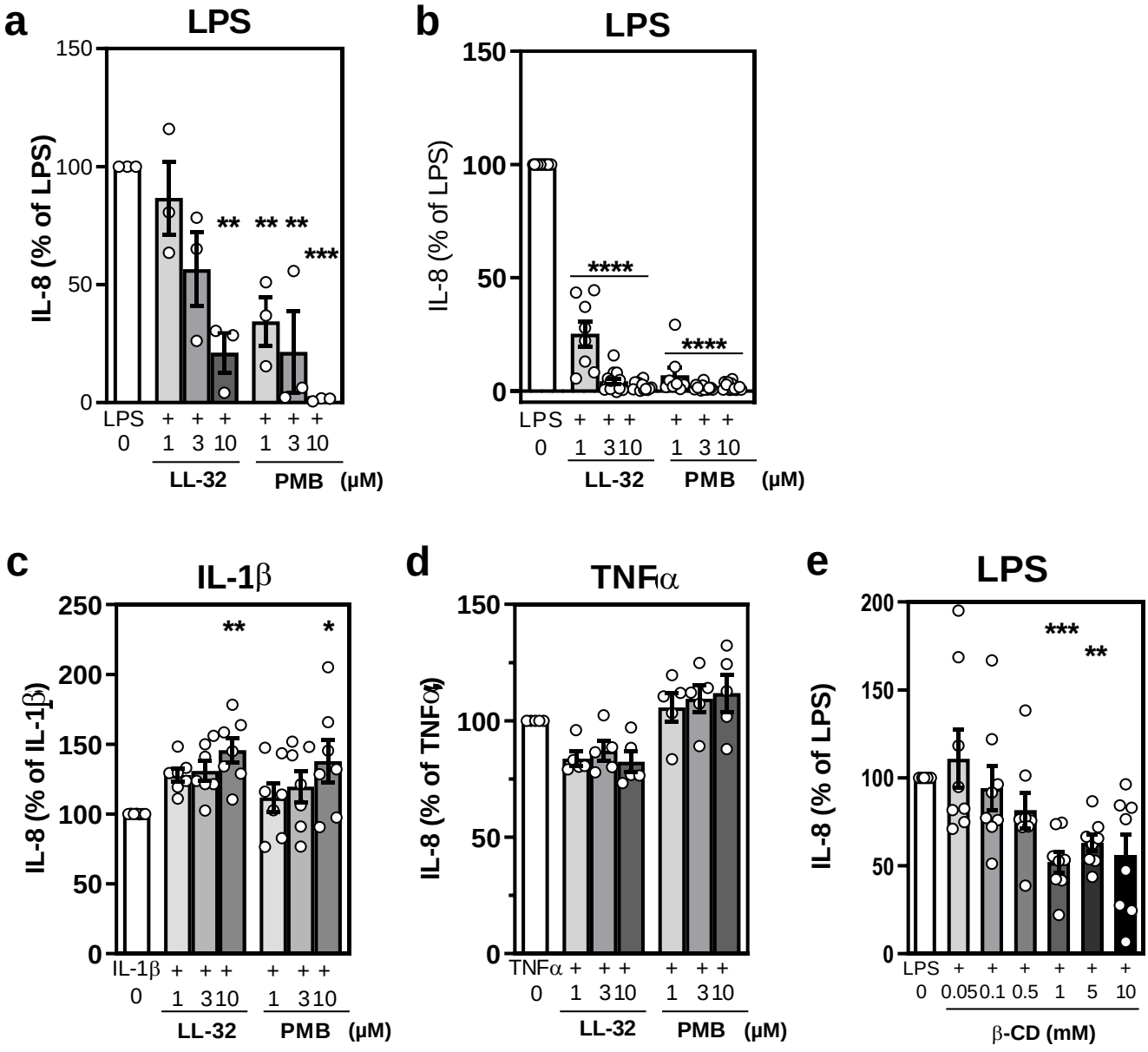
a
LPS
IL-8 (% of LPS)
150
100
50
0
** ** **
***
LPS + + + + + +
0 1 3 10 1 3 10
LL-32
PMB (μM)
b
LPS
IL-8 (% of LPS)
150
100
50
0
****
****
LPS + + + + + +
0 1 3 10 1 3 10
LL-32
PMB (μM)
c
IL-1β
IL-8 (% of IL-1β)
250
200
150
100
50
0
**
*
IL-1β + + + + + +
0 1 3 10 1 3 10
LL-32
PMB (μM)
d
TNFα
IL-8 (% of TNFα)
150
100
50
0
TNFα + + + + + +
0 1 3 10 1 3 10
LL-32
PMB (μM)
e
LPS
IL-8 (% of LPS)
200
150
100
50
0
***
**
LPS + + + + + +
0 0.05 0.1 0.5 1 5 10
β-CD (mM)

Figure 5

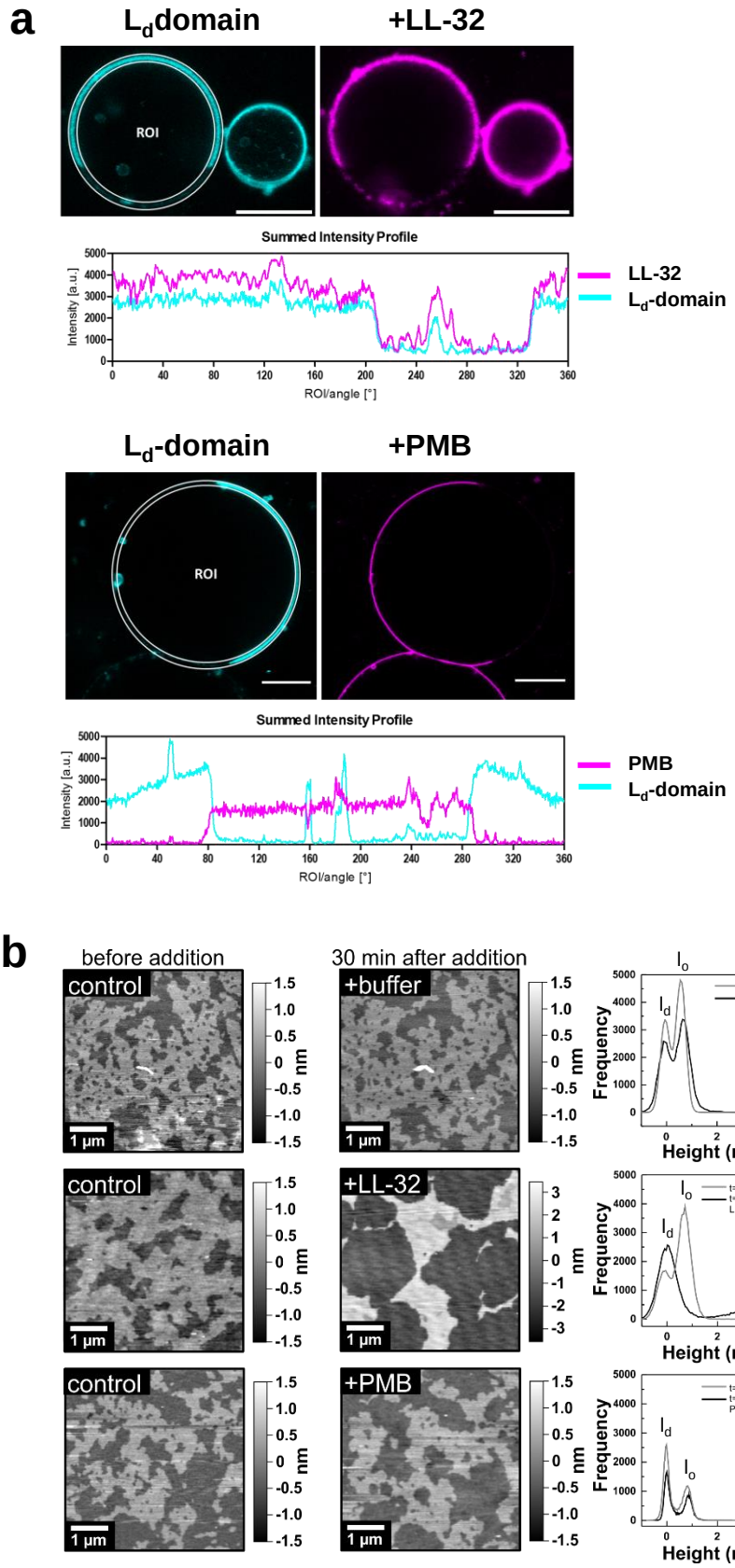
a
$L_d$domain
+LL-32
ROI
Summed Intensity Profile
Intensity [a.u.]
ROI/angle [°]
LL-32
L_d-domain
L_d-domain
+PMB
ROI
Summed Intensity Profile
Intensity [a.u.]
ROI/angle [°]
PMB
L_d-domain
b
before addition
30 min after addition
control
+buffer
+LL-32
+PMB
1 µm
nm
Frequency
Height (nm)
I_o
I_d
t=0 min
t=30 min
LL-32 addition
PMB addition

Figure 6

a

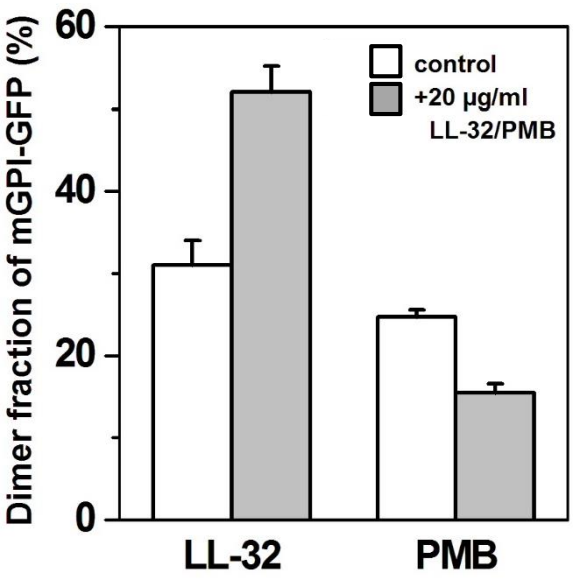
Dimer fraction of mGPI-GFP (%)
60
40
20
0
control
+20 µg/ml
LL-32/PMB
LL-32
PMB

b

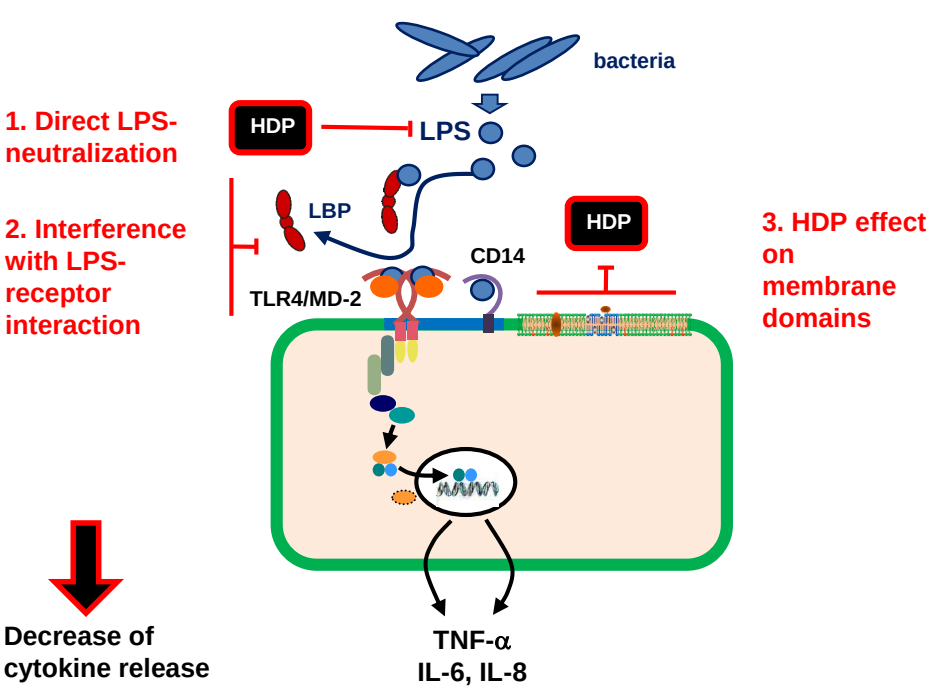
bacteria
1. Direct LPS-neutralization
HDP
LPS
LBP
2. Interference with LPS-receptor interaction
HDP
CD14
TLR4/MD-2
3. HDP effect on membrane domains
Decrease of cytokine release
TNF-α
IL-6, IL-8

Supplementary Table 1

Peptide	Origin	Amino acid sequence	MW ($g \cdot mol^{-1}$)
LL-32	human	LLGDFFRKSKEKIGKEFKRIVQRIKDFLRNLV-NH_2	3921.7
LL-37	human	LLGDFFRKSKEKIGKEFKRIVQRIKDFLRNLVPRTES-NH_2	4492.3
CAP18	rabbit	GLRKRLRKFRNKIKEKLKKIGQKIQGLLPKLAPRTDY-$CONH_2$	4432.5
CRAMP	murine	GLLRKGGEKIGEKLKKIGQKIKNFFQKLVPQPE-$CONH_2$	3749.5
BMAP-27	bovine	GRFKRFRKKFKKLFKKLSPVIPLLHL-$CONH_2$	3225.1
BMAP-28	bovine	GGLRSLGRKILRAWKKYGPIIVPIIRI-$CONH_2$	3073.9
hBD-3-l	human	GIINTLQKYYSRVRGGRSAVLSSLPKEEQIGKSSTRGRKSSRRKK-$CONH_2$	5063.6
NK-2	porcine	KILRGVCKKIMRTFLRRISKDILTGKK-$CONH_2$	3202.0
LPep19-2.5	synthetic	GCKKYRRFRWKFKGKFWFWG-NH_2	2712.2

Supplementary Table 2

Table S2: Gene-specific primers for cDNA amplification in real-time PCR; HPRT, hypoxanthine-phosphoguanine ribosyltransferase; UPL-probe #, universal-probe-library number (Roche Diagnostics).

Target gene	Primer	Sequence 5' – 3'	UPL-probe
HPRT	forward	tga cct tga ttt att ttg cat acc	# 73
	reverse	cga gca aga cgt tca gtc ct	# 73
TNF-α	forward	cag cct ctt ctc ctt cct gat	# 29
	reverse	gcc aga ggg ctg att aga ga	# 29
IL-1β	forward	tac ctg tcc tgc gtg ttg aa	# 78
	reverse	tct ttg ggt aat ttt tgg gat ct	# 78
IL-8	forward	aga cag cag agc aca caa gc	# 72
	reverse	atg gtt cct tcc ggt ggt	# 72

Supplementary Figure 1

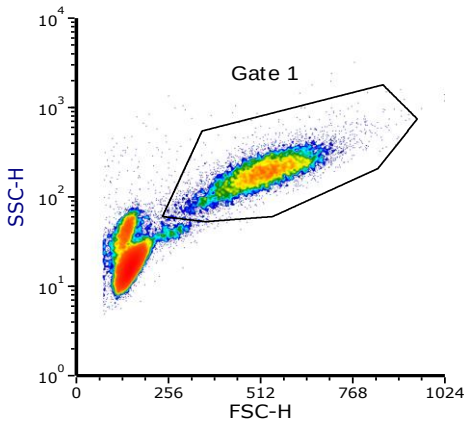

Supplementary Figure 2

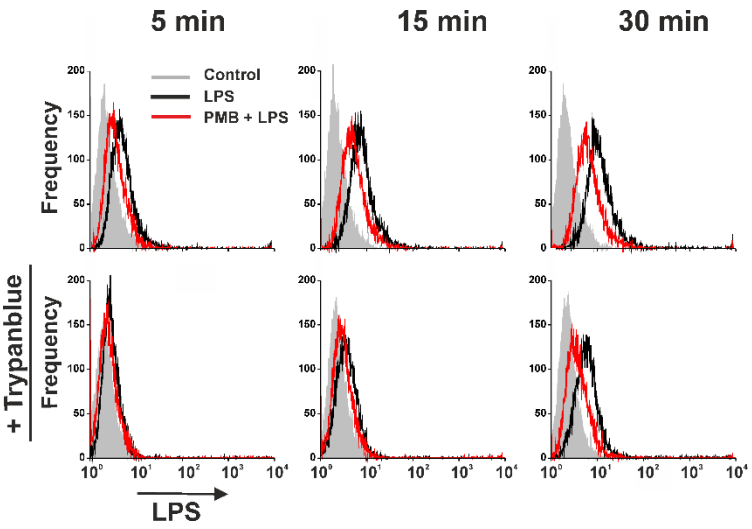

Supplementary Figure 3

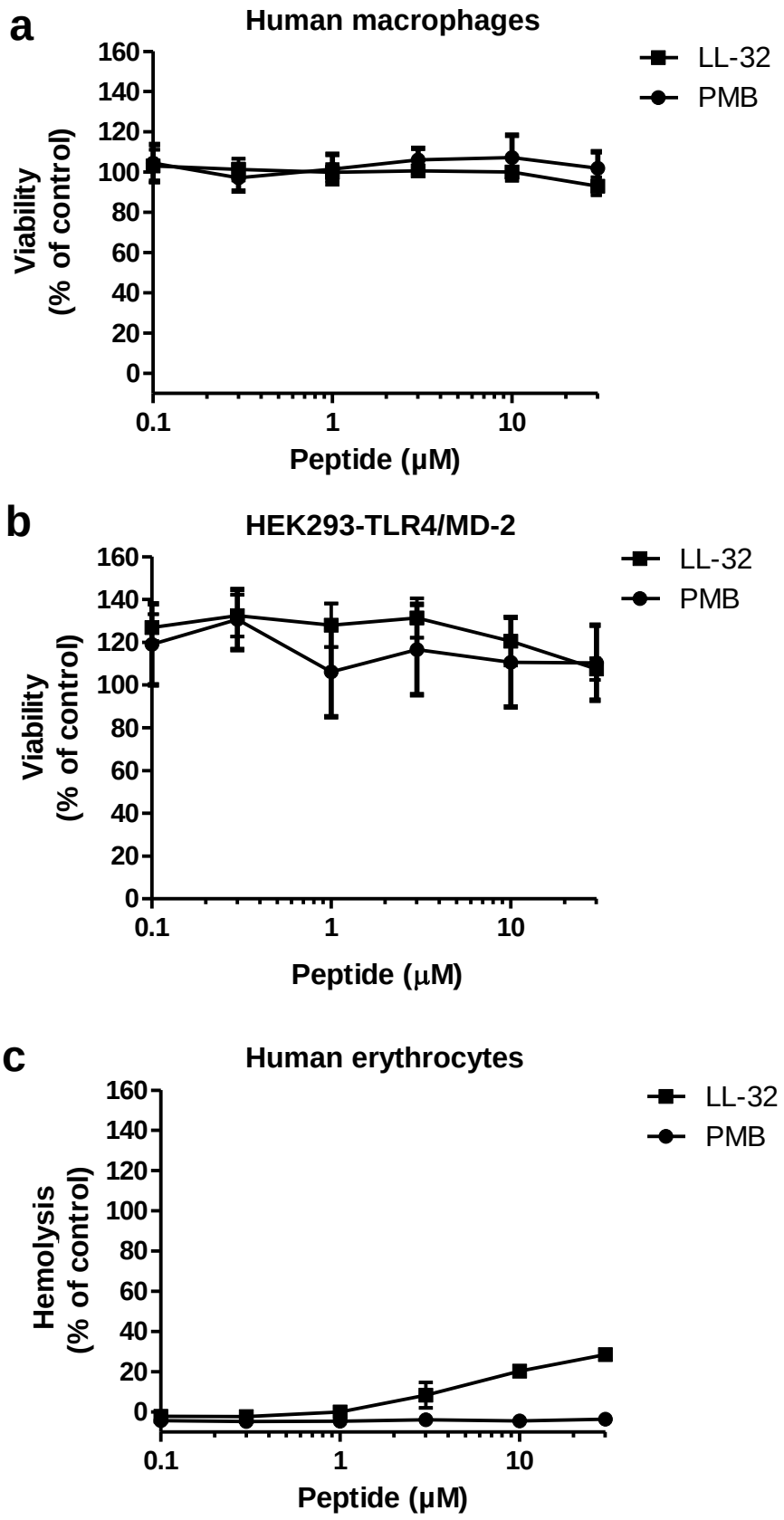

Supplementary Figure 4

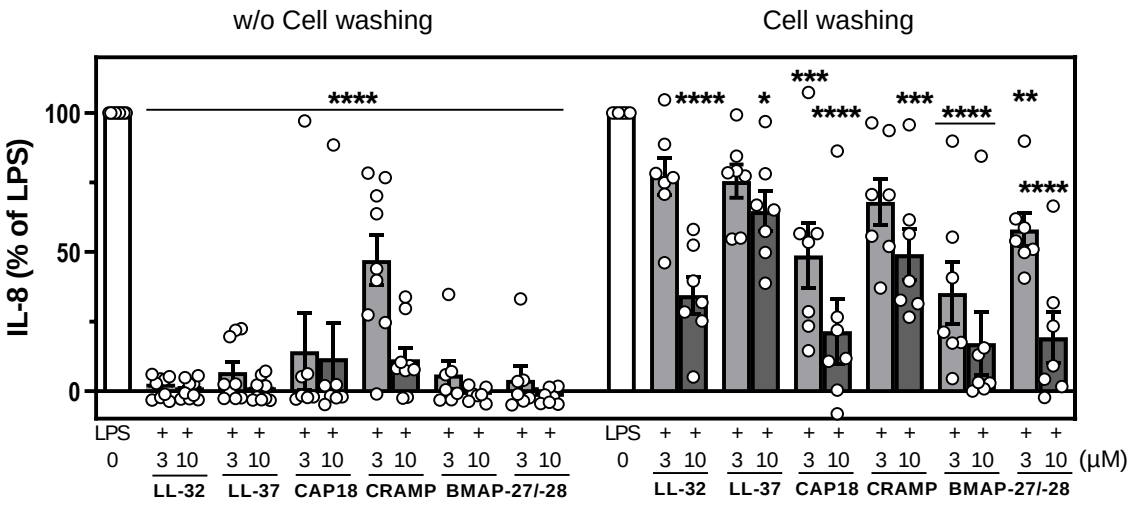

Supplementary Figure 5

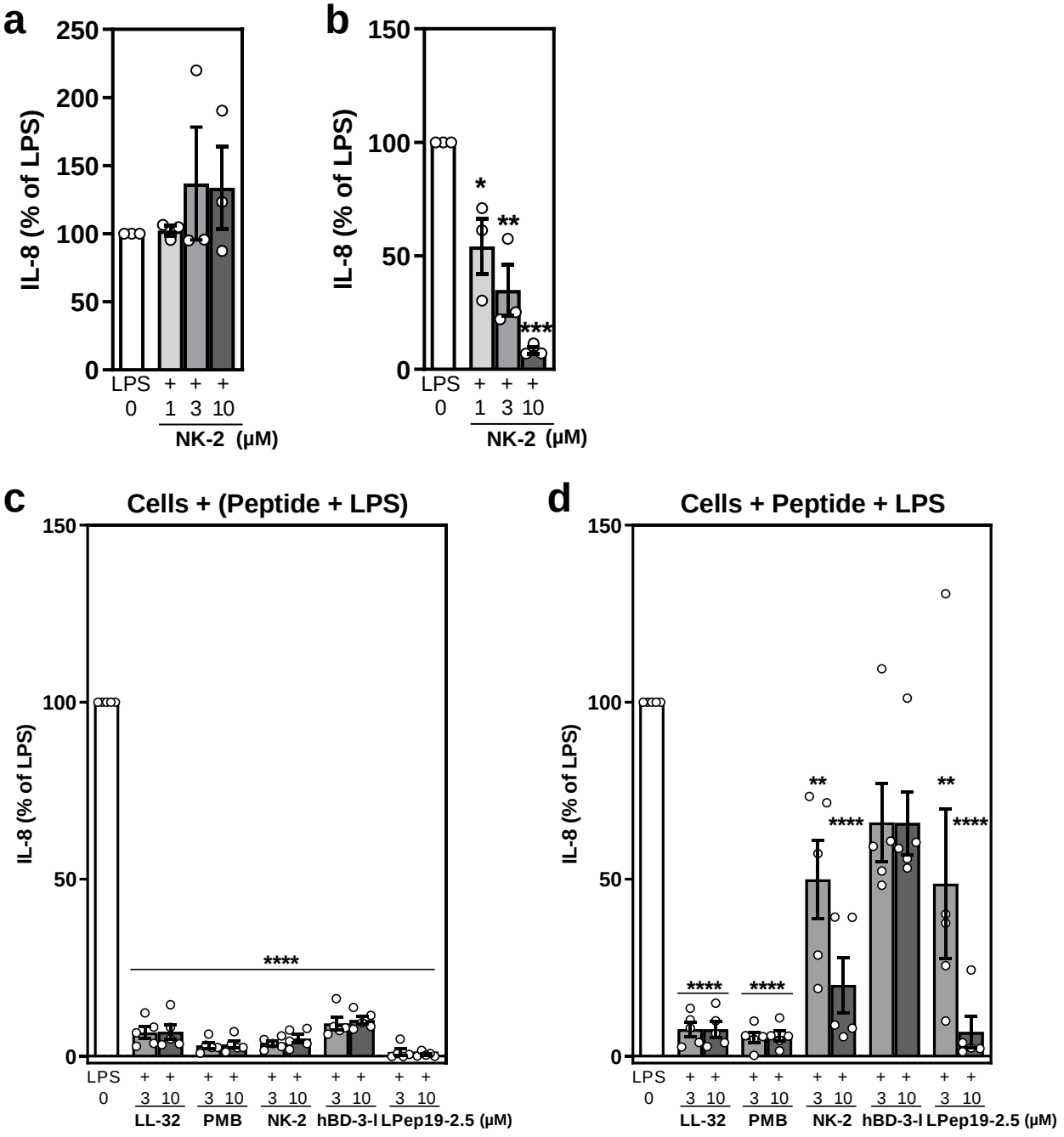

Supplementary Figure 6